ELSEVIER

Contents lists available at ScienceDirect

# European Journal of Medicinal Chemistry

journal homepage: www.elsevier.com/locate/ejmech



# Research paper



# Quantum mechanics-driven structure-activity relationship study of PEX5-PEX14 protein-protein interaction inhibitors based on a dibenzo [b,e] azepin-6(6H)-one scaffold

Michał Nowacki <sup>a,\*</sup>, Filipe Menezes <sup>b,\*\*</sup>, Emilia Pykacz <sup>a,c,d</sup>, Mateusz Popiołek <sup>a</sup>, Valeria Napolitano <sup>b,1</sup>, Chethan K. Krishna <sup>e</sup>, Vishal C. Kalel <sup>e</sup>, Ralf Erdmann <sup>e</sup>, Tony Fröhlich <sup>b</sup>, Oliver Plettenburg <sup>c,d</sup>, Michael Sattler <sup>b,f</sup>, Grzegorz M. Popowicz <sup>b,f,\*\*\*</sup>, Maciej Dawidowski <sup>a,\*\*\*\*</sup>

- <sup>a</sup> Department of Drug Technology and Pharmaceutical Biotechnology, Medical University of Warsaw, Banacha 1, 02-097, Warszawa, Poland
- b Institute of Structural Biology, Molecular Targets and Therapeutics Center, Helmholtz Munich, Ingolstädter Landstrasse 1, Neuherberg, 85764, Germany
- c Institute of Medicinal Chemistry, Molecular Targets and Therapeutics Center, Helmholtz Munich, Ingolstädter Landstrasse 1, Neuherberg, 85764, Germany
- d Center of Biomolecular Drug Research (BMWZ), Institute of Organic Chemistry, Leibniz Universität Hannover, Schneiderberg 1b, 30167, Hannover, Germany
- e Institute of Biochemistry and Pathobiochemistry, Department of Systems Biochemistry, Faculty of Medicine, Ruhr-University Bochum, 44780, Bochum, Germany
- <sup>f</sup> Bavarian NMR Center, Department of Bioscience, TUM School of Natural Sciences, Technical University of Munich, Lichtenbergstrasse 4, 85747, Garching, Germany

### ARTICLE INFO

### Keywords:

Protein-protein interaction inhibitors
Dibenzo[b,e]azepin-6(6H)-one
Trypanocidal inhibitors
Structure-based drug design
Multicomponent reactions
Quantum mechanical energy decomposition
and deconvolution analysis
Structure-activity relationship

# ABSTRACT

Targeting protein-protein interactions (PPIs) is a promising strategy in drug development. However, despite the considerable progress in the field, targeting PPIs with small molecules remains challenging, requiring novel strategies in inhibitor design and subsequent structure-activity relationship (SAR) studies. We have recently identified the PEX5-PEX14 PPI as a novel therapeutic target against diseases related to *Trypanosoma* infections and discovered small-molecule inhibitors against PEX14 using structure-based drug discovery (SBDD). The current study demonstrates that combining SBDD with quantum mechanical (QM) energy decomposition and deconvolution analysis (EDDA) provides an in-depth understanding of SAR in the newly developed PPI inhibitors class. We obtained diverse dibenzo[b,e]azepin-6(6H)-one PEX14 inhibitors, which resulted from redesigning the central scaffold of one of the previous compound lines and follow-up modifications. The diversification strategy yielded compounds obtained by multicomponent reactions (MCRs), from which the Kabachnik-Fields reaction products were the most potent tricyclic PEX5-PEX14 PPI inhibitors obtained so far. Overall, the activities of the compounds measured with biophysical assays aligned with the QM-derived compound binding energies. Hence, using an advanced computational approach, our results pave an alternative way for SAR rationalization of compounds against PPI targets.

# 1. Introduction

Protein complexes, the formation of which occurs through protein-

protein interactions (PPIs), are of particular significance for cellular processes such as inter- and intracellular transport, signal transduction, metabolism, growth, proliferation and apoptosis. Modulation of PPIs

### https://doi.org/10.1016/j.ejmech.2025.117979

Received 25 June 2025; Received in revised form 10 July 2025; Accepted 14 July 2025 Available online 18 July 2025

0223-5234/© 2025 The Authors. Published by Elsevier Masson SAS. This is an open access article under the CC BY-NC-ND license (http://creativecommons.org/licenses/by-nc-nd/4.0/).

<sup>\*</sup> Corresponding author. Department of Drug Technology and Pharmaceutical Biotechnology, Medical University of Warsaw, Banacha 1, 02-097, Warszawa, Poland \*\* Corresponding author. Institute of Structural Biology, Molecular Targets and Therapeutics Center, Helmholtz Munich, Ingolstädter Landstrasse 1, Neuherberg, 85764, Germany.

<sup>\*\*\*</sup> Corresponding author. Institute of Structural Biology, Molecular Targets and Therapeutics Center, Helmholtz Munich, Ingolstädter Landstrasse 1, Neuherberg, 85764, Germany.

<sup>\*\*\*\*</sup> Corresponding author. Department of Drug Technology and Pharmaceutical Biotechnology, Medical University of Warsaw, Banacha 1, 02-097, Warszawa, Poland

E-mail addresses: michal.nowacki@wum.edu.pl (M. Nowacki), filipe.menezes@helmholtz-munich.de (F. Menezes), grzegorz.popowicz@helmholtz-munich.de (G.M. Popowicz), maciej.dawidowski@wum.edu.pl (M. Dawidowski).

<sup>1</sup> Current affiliation: Institute of Biostructures and Bioimaging, National Research Council (CNR), Via Pietro Castellino, 111, 80131 Napoli, Italy.

can affect these processes in both beneficial and detrimental ways, making it an attractive strategy for developing new drugs against human diseases and designing molecular probes to better understand cellular events occurring in living organisms [1–4].

Considerable progress has been made in designing and developing new PPI modulators [5,6]. As a result, some PPIs have been successfully targeted by small molecules, providing new perspectives for therapies in important fields such as oncology [7], virology [8,9], immunology [10, 11], microbiology [12] and neuroregeneration [13]. Some of these compounds are now under clinical evaluation, but only a few (lifitegrast [14], venetoclax [15], tirofiban [16], carotegrast methyl [17], maraviroc and fostemsavir [9]) have entered the market so far [5,18]. Despite this remarkable progress, PPIs remain 'high-hanging fruits' in medicinal chemistry. Their modulation offers an attractive strategy to tackle complex biochemical processes, but, for several reasons, they remain very challenging to address by small molecules. In particular, proteins interact primarily via small and shallow binding pockets that are non-uniformly distributed over extended, flat, solvent-exposed surfaces. This starkly contrasts with 'more typical', druggable protein targets such as enzymes and GPCRs, which have deeper and less solvent-accessible binding sites for small molecular ligands. Further, the binding events in the PPI interface hotspots are usually hydrophobic and aromatic, posing a serious challenge for developing compounds with optimal pharmacochemical profiles. [1,19]. Consequently, there is a need to search for new methods to facilitate PPI inhibitor design and help understand their complex structure-activity relationship (SAR).

The PEX5 and PEX14 protein complex formation is essential to glycosome biogenesis in the Trypanosomatidae family: they import cytosolic enzymes into this organelle. We have previously shown that disrupting their PPI offers a novel strategy for developing antiparasitic agents [20]. The PEX5-PEX14 PPI is an example of a very challenging molecular target. PEX5 binds the N-terminal domain (NTD) of PEX14 with its repeated, helical WxxxF/Y motifs ('x' denotes any non-proline amino acid, Fig. 1A). In these sequences, the aromatic, hydrophobic W and F/Y sidechains are projected along one face of the helix, towards their respective Trp and Phe/Tyr binding pockets (hotspots) in the PEX14 surface. The Trp hotspot is reasonably deep, while the Phe/Tyr pocket is shallow and highly solvent-exposed [21]. An important feature of the PEX5-TbPEX14 PPI interface is the occurrence of the  $\pi$ -stacked F17 and F34 side chains that form a hydrophobic, aromatic 'bridge' separating the two binding pockets in the TbPEX14 surface (Fig. 1AB). Hence, the nature of this target is highly lipophilic, and only several polar amino acid residues may be of use for ligand design (i.e., N13, E16, D20, R22, T26, S30, K38) that occur on the rim of the hydrophobic

hotspots (Fig. 1B) [22].

In our previous efforts to address this challenging molecular target, we developed several chemical classes of inhibitors: pyrazolo[4,3-c] pyridines 1 obtained by the 3D pharmacophore screening [22]; 2,3,4, 5-tetrahydrobenzo[f] [1,4]oxazepines 2 designed using the chemically advanced template search (CATS) algorithm [23]; and oxopiperazine-based mimetics of PEX5 WxxxF motif 3 [24] (Fig. 2A). Although these compounds were developed by different structure-based drug discovery (SBDD) approaches and belong to distinct chemical classes, they all share a common binding mode to PEX14, with aromatic rings addressing the hydrophobic Trp and Phe pockets and the central core shielding the  $\pi$ -stacked F17 and F34 side chains. Additionally, some water-mediated contacts with polar residues in the PEX5-PEX14 PPI interface are crucial for compound binding and creating the optimal water shell around the ligand-protein complex [25].

Another class of PEX5-PEX14 PPI inhibitors emerged from a highthroughput screening (HTS) campaign employing AlphaScreen [27] and NMR biophysical assays [28]. These compounds were based on benzo[b]pyrido[3,2-f] [1,4]thiazepin-5(6H)-one 4, dibenzo[b,f] [1,4] thiazepin-11(10H)-one 5 and dibenzo[b, f] [1,4]oxazepin-11(10H)-one 6 cores and constituted interesting tricyclic frameworks for targeting the two-aromatic hotspot system in the PEX14 surface of the PEX5-PEX14 PPI (Fig. 2B). The co-crystal structure of inhibitor 5 with TcPEX14 NTD (PDB accession code: 7QRC, Fig. 3A) showed that the compound mimics the positioning of aromatic residues of PEX5 native WxxxF motifs in their respective hotspots on the PEX14 surface (Fig. 3B). Thus, the terminal benzene ring of the dibenzo[b,f] [1,4]thiazepin-11 (10H)-one 6-7-6 system in compound 5 is in approximately the same spatial orientation as the phenyl group of the Phe residue of the PEX5 WxxxF motif, while the aromatic moiety attached to the C-7 position of the tricyclic system through an acetamide linker overlaps with the indole portion of Trp side chain of the WxxxF repeat. A critical feature of the tricyclic system in 5 is its bent conformation, which allows for the proper positioning of the terminal benzene ring in the Phe hotspot as well as for the effective shielding of the diaromatic F16-F33 bridge of TcPEX14 by a second aromatic ring.

Importantly, our previous experiences in SBDD targeting the flat PEX14-PEX5 PPI interface show that even slight activity improvements within the respective compound lines are not readily achievable. Moreover, the SAR rationalization is particularly challenging because the experimental binding results do not always match expectations based on the structural data and docking. We present a hybrid classical SBDD-quantum mechanics (QM) approach to address this. We perform the design, synthesis, biophysical evaluation and an in-depth, systematic

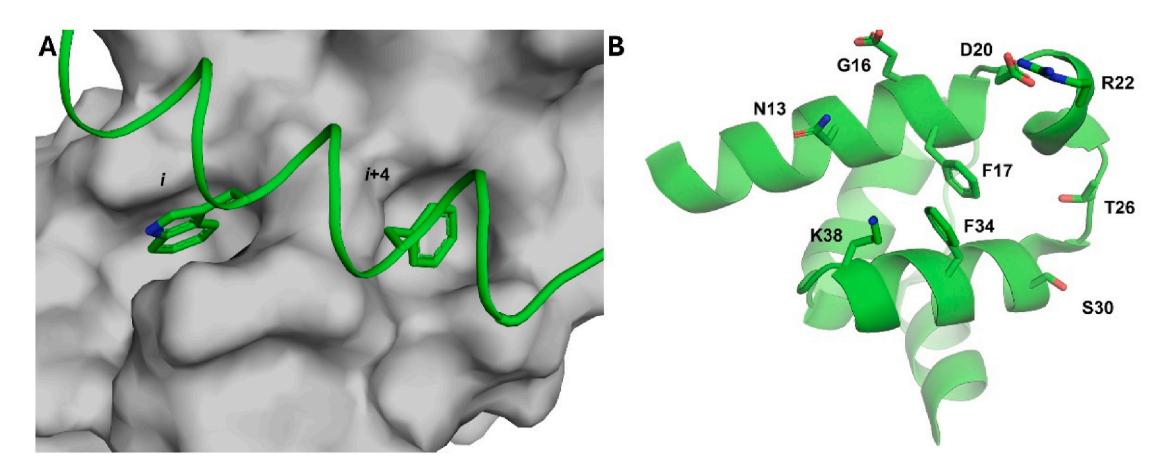


**Fig. 1.** Structural features of the PEX5–PEX14 PPI. A) Binding mode of PEX5  $\alpha$ -helix fragment (green) to *Hs*PEX14 NTD (light gray) derived from an NMR structure (PDB accession code: 2W84). The Trp and a Phe hotspots in the PEX14 surface are filled with *i* and *i*+4 aromatic amino acid side chains of the PEX5 WxxxF motif, respectively. B) The structure of the *Tb*PEX14 NTD was adopted from a protein-ligand co-crystal structure (PDB accession code: 5L87). The parallel-displaced  $\pi$ -stacked benzene rings of F17 and F34 side chains separate the Trp and Phe pockets. Polar amino acid side chains on the rim of the PEX5-PEX14 PPI interface are shown. (For interpretation of the references to color in this figure legend, the reader is referred to the Web version of this article.)

Fig. 2. Previously developed chemical classes of PEX5-PEX14 PPI inhibitors. A) Examples of pyrazolo[4,3-c]pyridine 1, 2,3,4,5-tetrahydrobenzo[f] [1,4]oxazepine 2 and dibenzo[b,f] [1,4]oxazepin-11(10H)-one 3 derivatives. B) Examples of tricyclic benzo[b]pyrido[3,2-f] [1,4]thiazepin-5(6H)-one 4, dibenzo[b,f] [1,4]thiazepin-11(10H)-one 5 and dibenzo[b, f] [1,4]oxazepin-11(10H)-one 6 derivatives. All these compounds belong to the class C (structural mimetics, 3) and class D (mechanistic mimetics, 1,2,4-6) of peptidomimetics, according to the classification proposed by Pelay-Gimeno and co-workers [26]. The common binding modes are illustrated: the aromatic residues mimic the native binding of PEX5 WxxxF fragments to PEX14 Trp and Phe pockets, and the central core (bold) interacts with the solvent-exposed F17 and F34 residues. The potencies of PEX5-TbPEX14 PPI disruption and cytotoxic effects against T. brucei are shown for compounds 1–3. The activity data of tricyclic inhibitors 4–6 are shown in Table 1.

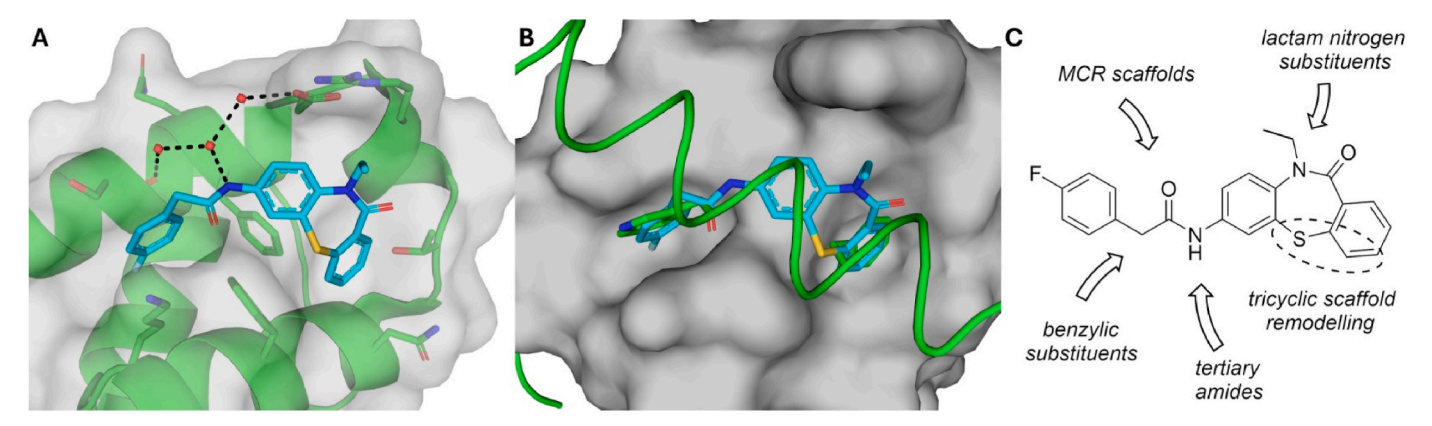


**Fig. 3.** The binding mode of the tricyclic dibenzo[ $b_f$ ] [1,4]thiazepin-11(10H)-one inhibitor **5.** A) The high-resolution co-crystal structure of compound **5** with TcPEX14 NTD (PDB accession code: 7QRC). The tricyclic 6-7-6 system of the inhibitor adopts a bent conformation, which allows for addressing the Phe hotspot of TcPEX14 and shielding of the diaromatic bridge. B) Comparison of the binding pose of compound **5** at the binding site of TcPEX14 NTD and the PEX5 WxxxF motif with HsPEX14 NTD (PDB accession code: 2W84). The inhibitor mimics the spatial orientation of the aromatic residues in native WxxxF motifs. C) Synthetically plausible structural modifications of compound **5** for an in-depth SAR study.

QM-assisted SAR analysis of novel benzo[b]pyrido[2,3-e]azepin-5(5H)one and dibenzo[b,e]azepin-6(6H)-one inhibitors that result from a -S-(or -O-) to -CH<sub>2</sub>- transition in the middle fragment of the 6-7-6 systems in compounds 4-6 and follow-up structural modifications. In this study, we combine SBDD with an advanced quantum mechanical Energy Decomposition and Deconvolution Analysis (EDDA), which partitions binding interaction energies over several intermolecular forces and factorizes each contribution with atomic granularity. The proposed method aims at a more detailed compound-protein interaction analysis than the one derived from analysis of docking scores, rationalizing the atoms and functional groups responsible for forming the ligand-protein complex. Consequently, it guides an in-depth SAR rationalization. The base premise of our analysis is that structural data on ligand-protein complexes results from a delicate balance of physicochemical forces - electrostatics, lipophilicity, steric repulsion, charge transfer, etc. - leading to a thermodynamic stabilization of the small molecule in the protein's pocket. This effect, driven primarily by a favorable binding enthalpy, is decoded using the EDDA algorithm. Importantly, if a good understanding of the binding drivers is sought, an in-depth decomposition and a visual representation of the most relevant atomic participants are needed.

# 2. Results and discussion

# 2.1. Remodeling of the tricyclic scaffold

We initiated our study by comparing the positioning of the tricyclic scaffold of the previously studied compound 5 with that of its newly designed -CH<sub>2</sub>- analog 7 in the PEX5-PEX14 PPI interface [28]. We docked compound 7 to TbPEX14 and overlaid the resulting pose with that of compound 5 in its cocrystal with TcPEX14 (PDB accession code: 7QRC, Fig. 4). We observed an overall excellent agreement between these two binding poses. To further verify the design of analog 7, we experimentally evaluated its capability to disrupt the PEX5-TbPEX14 PPI. Propitiously, the compound inhibited the complex formation between the PEX5-derived peptide (amino acid sequence: ALSENWAQE-FLA) and TbPEX14, with an EC<sub>50</sub> of 95  $\mu$ M in the AlphaScreen proximity-based biophysical assay (Table 1). Propitiously, this corresponds to a two-fold activity gain over the previously reported derivative 5 and almost an order of magnitude improvement with respect to the oxygen analog 6 [28].

We have also remodeled the terminal part of the tricyclic system in 7. This effort was driven by the fact that one of the previously obtained active hits, compound 4, contained a pyridine ring instead of a benzene ring in the terminal fragment of its 6-7-6 ring system [28]. Therefore, we

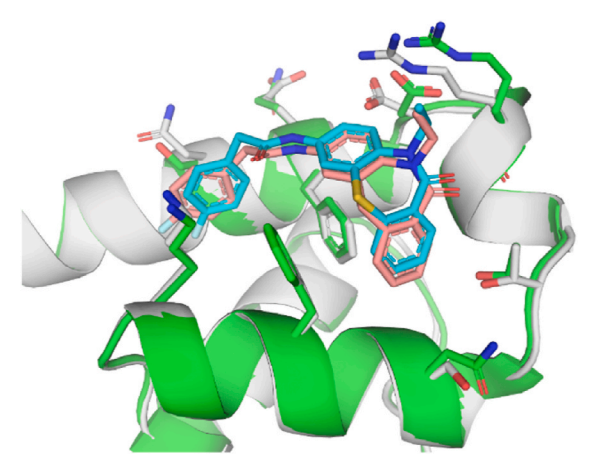


**Fig. 4.** Comparison of the binding pose of compound **7** (pink) docked to *Tb*PEX14 (green) with the binding mode of compound **5** (blue) derived from its co-crystal with *Tc*PEX14 (silver, PDB accession code: 7QRC). A high degree of similarity is observed between these two binding poses. (For interpretation of the references to color in this figure legend, the reader is referred to the Web version of this article.)

investigated whether a similar modification of the tricyclic scaffold applied to compound 7 could affect  $\mathit{Tb}$ PEX14 binding by improving  $\pi$ -stacking interactions. To this end, we synthesized analog 8. However, when tested in the AlphaScreen assay, the compound displayed a three-fold decrease in potency for disrupting the PEX5- $\mathit{Tb}$ PEX14 PPI (EC<sub>50</sub> = 301  $\mu$ M), compared to the parent compound 7.

The experimentally measured activities of compounds 5–8 cannot be rationalized by analyzing their docking poses to TbPEX14. Therefore, to better understand the origins of the pronounced differences in protein binding, we performed a quantum mechanical (QM) analysis of binding using our Energy Decomposition and Deconvolution Analysis (EDDA). EDDA is a QM-based partition scheme, which calculates and factorizes binding energies over several components, each of which is associated with a specific physicochemical force: electrostatic interactions (ES), polarization (POL), charge transfer (CT), lipophilicity or dispersion (DISP), steric hindrance or electronic repulsion (REP), and solvation contributions (SOLV). All these terms are additive and sum up to the interaction or binding energy (INT). Because the binding energy correlates with the binding enthalpy, this partitioning identifies the driving forces that lead to the binding. Overall, the EDDA calculations for derivatives 5-8 (Fig. 5, S1A-E, Table S1) show a good correlation between the calculated binding energies and the experimental EC50 values obtained from the AlphaScreen assay (Fig. S1A).

We first rationalized the weaker binding of compound 5 with respect

to 7. In the decomposed energies, we see a stronger capability of 5 to engage in electrostatic interactions with *Tb*PEX14 (Fig. 5B). Interestingly, despite the larger van der Waals radius of a sulfur atom compared to a carbon atom, compound 5 experiences less electronic density repulsion than derivative 7 (Fig. 5B), which we attribute to the lack of hydrogen atoms removed with the methylene group. The changes in lipophilic interactions, dispersion and polarization interactions are also of similar magnitude with respect to one another, and of opposite sign, leading to a cancellation of effects. The stabilizing effect of electrostatics is observed in 5. However, it is overcompensated by the negative solvation contributions, which eventually leads to a slightly less favorable binding energy of the compound with respect to analog 7 (Fig. 5B–Table 1).

The EDDA calculations performed for the complexes of compounds 6 and 7 with TbPEX14 showed the positive impact of the oxygen atom of the tricyclic system in the former derivative for the overall electrostatic interactions (Fig. 5C). This is particularly interesting because this atom is positioned in a lipophilic sub-pocket of the PEX5-PEX14 PPI interface, and the protein has an overall negative charge of -1. This indicates that the oxygen is located in a positively charged chemical environment, most likely conferred by the R22 and K38 residues. On the other hand, because this oxygen is placed in a lipophilic sub-pocket of TbPEX14, the overall effect resulting from solvation of this compound is detrimental for binding when compared to the -CH<sub>2</sub>- analog 7 (Fig. 5B). The repulsion contributions follow the expected trend, as replacing the -CH2group with oxygen negatively affects the overlap of electronic densities (Fig. 5B). This density overlap is similarly reflected in the polarization contributions of derivatives 6 and 7. Expectedly, the transition from -CH<sub>2</sub>- to -O- negatively influences dispersion contributions (Fig. 5B). Overall, the influence of the oxygen atom on the binding of compound 6 to TbPEX14 is negative (Fig. 5D) because it weakens lipophilic interactions and provides a slightly worse shape complementarity to the pocket, with respect to analog 7.

When comparing compounds 7 and 8, we would expect the EDDA results to be similar to those obtained for compound 6 because of the additional electronegative nitrogen atom in its tricyclic core. However, the chemical profile of compound 8 in the PEX5-PEX14 PPI interface has a slightly negative impact on electrostatic interactions (Fig. 5B). Still, electrostatics are strongly attractive, which indicates the positively charged environment in which this nitrogen atom is also placed (Fig. 5C). The solvation terms are also negatively influenced, just like in the case of compound 6 (Fig. 5B). The major differences in the binding contributions of 7 and 8 result from polarization, repulsion, and dispersion effects. The change in repulsion is negative, which shows less contact between electronic densities. On the contrary, the reduced contact of electronic densities leads to fewer polarization effects upon binding and less dispersion (Fig. 5B). Overall, the transition from CH to

**Table 1** Remodeling of the tricyclic scaffold.

#	-X-	-Y-	<i>Tb</i> PEX14 EC <sub>50</sub> [μM] <sup>a</sup>	T. brucei EC <sub>50</sub> [μM] <sup>b</sup>	<i>HepG2</i> EC <sub>50</sub> [μM] <sup>b</sup>	SI <sup>c</sup>
5	CH	S	230 <sup>d</sup>	5.40 (4.76-6.12)	ND	-
6	CH	О	875 <sup>d</sup>	8.12 (7.41-8.94)	ND	-
7	CH	$CH_2$	94	7.2 (6.5–7.9)	>100	>13.8
8	N	$CH_2$	301	15 (12–19)	>50	>3.6

 $<sup>^{</sup>a}$  EC50 values were calculated as a Hill curve fit to 12-point titration (n = 4), with SD mostly within 20 %.

<sup>&</sup>lt;sup>b</sup> EC<sub>50</sub> values are shown as mean (n = 4). Values in parentheses are 95 % confidence intervals. ND-not determined.

<sup>&</sup>lt;sup>c</sup> The selectivity index is calculated as HepG2 EC<sub>50</sub>/T. brucei EC<sub>50</sub>.

d Data taken from ref. [28].

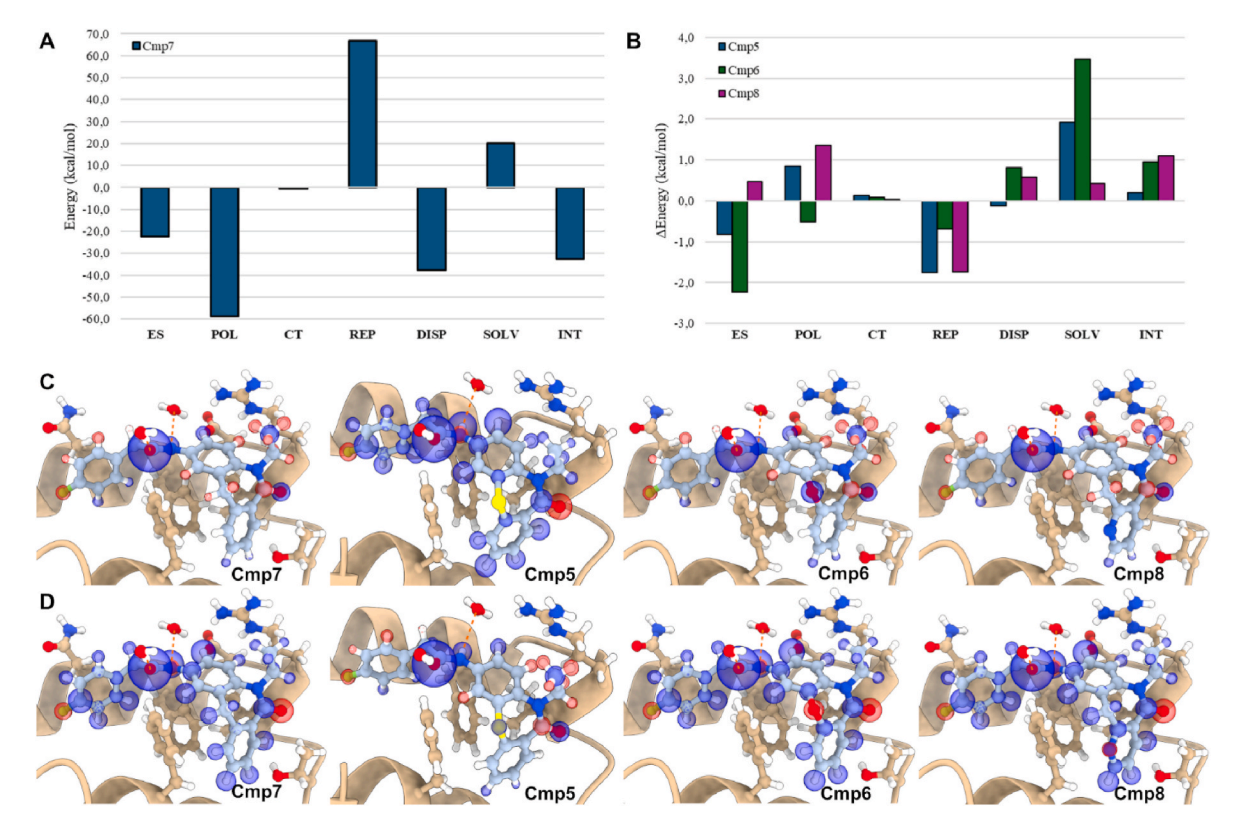


Fig. 5. The QM-EDDAs for the interactions of compounds 5–8 with *Tb*PEX14. A) Column plot of the decomposed interaction contribution energies of a reference compound 7 with *Tb*PEX14. B) Column plots of differences in the decomposed interaction contribution energies of analogs 5, 6, and 8 with *Tb*PEX14, with respect to those of the reference compound 7. C) The ES maps for binding modes of compounds 7 (first), 5 (second), 6 (third), and 8 (last) to *Tb*PEX14. D) The INT maps for binding modes of compounds 7 (first), 5 (second), 6 (third), and 8 (last) to *Tb*PEX14. The maps are illustrations of the respective energy contributions of each of the ligand atoms. Blue spheres represent attractive interactions, whereas red spheres indicate repulsive atomic contacts. The size of each sphere correlates with the strength of the respective interaction. Only the maps showing the most important contributions are shown here. All maps for compounds 5–8 are provided in Supplementary Data B (Fig. S1B–E). (For interpretation of the references to color in this figure legend, the reader is referred to the Web version of this article.)

N in the terminal aromatic ring has a negative impact on the binding of 8 to *Tb*PEX14, as seen in the total interaction maps (Fig. 5D). Such a prediction is only possible because the QM analyses are based on the electronic density properties of each chemical group and would have likely been missed using classical SBDD methods.

Having a strong experimental and computational indication that the newly designed dibenzo [b,e] azepin-6(6H)-one scaffold of compound 7 can be a valuable source of new PEX5-PEX14 PPI inhibitors, we proceeded with a systematic, in-depth SAR study (Fig. 3C). Using the available structural information on the possible ligand-protein interactions and considering the synthetic feasibility of the target derivatives, we have identified two plausible modification sites in 7: the cyclic amide of the middle ring in the 6-7-6 system and the exocyclic aniline nitrogen atoms.

# 2.2. SAR study of the lactam substituents

To analyze the effect of the cyclic amide substitution on PEX5-*Tb*PEX14 PPI inhibitory properties, we have synthesized a small subset of compounds 9–13 with various aliphatic residues in this position (Table 2). In general, we have found that the aliphatic substituents attached to the amide nitrogen atom critically impact *Tb*PEX14 binding. This was best illustrated by the fact that the activity of the unsubstituted derivative 9 dropped nearly fivefold (EC $_{50} = 562~\mu$ M), whereas analogs 10 and 11, with methyl or isopropyl substituents, disrupted the PEX5-*Tb*PEX14 PPI with a similar potency as the ethyl derivative 7 (EC $_{50} = 153~\mu$ M and 118  $\mu$ M, respectively). According to our docking results of 7 to *Tb*PEX14 shown in Fig. 4, the lactam group of the tricyclic core points towards the aliphatic part of the R22 side chain in the PEX5-*Tb*PEX14

**Table 2** SAR of the lactam substituents.

#	R	TbPEX14 EC <sub>50</sub> [μM] <sup>a</sup>	T. brucei EC <sub>50</sub> [μM] <sup>b</sup>	<i>HepG2</i> EC <sub>50</sub> [μM] <sup>b</sup>	SI <sup>c</sup>
7	-1-	95	7.2 (6.5–7.9)	>100	>13.8
9	H - † -	562	23 (18–28)	>100	>4.3
10	-/-	153	9.3 (8.1–10.7)	>100	>10.7
11	7	118	7.2 (5.9–8.5)	>100	>13.8
12	- F-COOEt	234	5.1 (4.4–5.8)	7.6 (6.0–12.5)	1.5
13	-	>1000	4.6 (4.2–5.1)	>100	>21.7

 $<sup>^{\</sup>rm a}$  EC  $_{50}$  values were calculated as a Hill curve fit to 12-point titration (n = 4), with SD mostly within 20 %.

 $<sup>^{</sup>b}$  EC  $_{\!50}$  values are shown as mean (n = 4). Values in parentheses are 95 % confidence intervals.

 $<sup>^{\</sup>rm c}\,$  The selectivity index is calculated as HepG2 EC50/T. brucei EC50.

PPI interface. Consequently, the aliphatic substituents attached to this exit vector likely form lipophilic contacts with this residue. This explanation is further supported by analyzing the structural features of the PEX5-PEX14 PPI [21]. Frequently, the i+4 (F) residues of the PEX5 WxxxF motifs are followed by an L, the aliphatic side chain of which points towards the hydrophobic part of R22 of PEX14. This interaction seems essential since in the peptide scan of short PEX5-derived sequences presented in the same publication [21], the replacement of L was restricted only to other hydrophobic residues (e.g., I or A). Consequently, the aliphatic residues attached to the lactam nitrogen of 7, 10, and 11 mimic the placement of an aliphatic side chain in the native PEX5-PEX14 PPI (Fig. S2A). We have also attempted to address the polar guanidinium part of the R22 side chain and synthesized the ethoxycarbonylmethyl derivative 12. However, this compound was not superior when compared to its close analogs 7, 10 or 11 (EC50 = 234  $\mu$ M).

One of the attempts to synthesize inhibitor 7 resulted in the formation of the *O*-regioisomer byproduct that eventually enabled us to obtain the *O*-ethyl derivative 13. Although the binding mode of tricyclic inhibitors to *Tb*PEX14 excludes the occurrence of steric clashes of derivative 13 with protein residues, this compound did not disrupt PEX5-*Tb*PEX14 PPI at concentrations up to 1 mM. Moreover, the QM-optimized structure of compound 13 adopts a bent conformation required for *Tb*PEX14 binding (Fig. S2B). On the other hand, the calculations show that the partial charge on the oxygen atom in compound 13 is halved upon ethylation when compared to the *N*-alkyl amide analog 7 (-0.28 vs -0.54, respectively). Likely, this leads to the depolarization of the solvent-exposed lactam fragment of inhibitor 13, thus a weaker protein binding is observed.

### 2.3. SAR study of the exocyclic nitrogen substituents

Concluding the results of the tricyclic scaffold manipulation and exploring the role of the substituents in the cyclic lactam, we observed a strong preference of the PEX5-*Tb*PEX14 PPI interface for lipophilic interactions. Further, the presence of functional groups and atoms that engage in electrostatic interactions in these inhibitor fragments negatively influences the binding. Therefore, the major challenge in balancing the hydrophobic character of *Tb*PEX14 ligands lies in the correct placement of electrostatics-engaging functional groups. We varied residues attached to the exocyclic aniline nitrogen atom with this aim. Multiple modifications are possible at this exit vector, and we envisioned that they might enhance the ligand hydrophobic contacts with *Tb*PEX14 (e.g., through variations of the lipophilic, aromatic substituents targeting the Trp pocket). They also may alter favorable, direct, and water-mediated polar interactions with the nearby amino acid side chains (i.e., with N13, E16, D20, R22, K38).

# 2.3.1. SAR of the tertiary amides

We first investigated the effects of substituting the exocyclic amide nitrogen in 7 with simple alkyl groups (Table 3), some of them having additional terminal, hydrophilic groups to explore possible polar interactions with the protein. Although we did not anticipate that this type of structural modification would generate steric clashes with the protein residues, we observed that, in general, the inhibitory activity of the designed compounds 14-16 was significantly diminished (no activity at concentrations up to 1 mM for 14 and 15,  $EC_{50}=273~\mu M$  for 16). We attributed this to the possible interference of the introduced substituents with the ligand solvent shell. As seen in all inhibitor-PEX14 cocrystal structures obtained so far, the amide hydrogen of the inhibitor located in this region of the PEX5-PEX14 PPI interface can participate in important water-mediated connections with the polar amino-acid residues neighboring the Trp pocket, thus stabilizing the complex [22,25,28]. In compounds 14-16, the hydrogen atom of 7 was replaced by alkyls, which likely disturbed these interactions, e.g., by promoting a reorientation of the exocyclic amide group. However, it should be noted that, contrary to derivatives 14 and 15, analog 16 retained some of the activity of the unsubstituted parent compound 7.

We performed docking experiments and EDDA calculations for compounds 14-16 (Fig. 6, S3A-D and Table S3). Overall, the calculated binding energies correlate well with the experimental affinities (Fig. S3A). Considering the importance of explicit water molecules used in docking, during the computational experiments we postulated that introducing the alkyl groups in the exocyclic amide as in derivatives 14–16 would primarily induce a pronounced change in the binding mode of the ligands, followed by subsequent minor rearrangements of the water-mediated interactions with protein residues to accommodate the introduced residues. Indeed, to still fit the PEX5-PEX14 PPI interface, the exocyclic amide residues of these derivatives had to readjust and rotate by 180° (in compounds 14 and 16) or by 90° (in ligand 15), with respect to the conformation observed in the binding pose of the parent inhibitor 7. This rearrangement led to the disruption of hydrogen bonds with water molecules in derivative 15. In the case of compound 14, one hydrogen bond was broken, whereas the ester analog 16 could retain the two hydrogen bonds.

These events and their effects on binding can be followed in the respective EDDA maps for each ligand-protein complex. The electronic repulsion maps, which indicate close electronic density contacts, show that in the complex of compound 14 with *Tb*PEX14, one hydrogen bond is formed by the amide carbonyl oxygen and one of the water molecules. However, forming this interaction forces the *N*-methyl substituent to point towards the second water molecule (Fig. 6B–I). The total interaction maps show an overall repulsive interaction, illustrated by the red sphere surrounding the methyl group (Fig. 6C). Consequently, and contrary to the reference compound 7, the ligand-protein electrostatic interactions are repulsive (Fig. 6A). Though the solvation terms somewhat compensate the electrostatic destabilization, the increase in electronic density repulsion with the solvation sphere of the complex explains well the loss of binding of ligand 14 (Fig. 6B).

The electronic repulsion maps of the 2-hydroxyethyl analog 15 indicate several strong, close contacts scattered all over the ligand-protein interaction surface. This observation seems odd at first because the local binding mode of the tricyclic 6-7-6 system and the fluorophenyl group remains somewhat conserved between compounds 7, 14, and 15. However, all interaction maps are normalized with respect to the strongest atomic contact for each interaction.

**Table 3** SAR of the tertiary amides.

#	R	<i>Tb</i> PEX14 EC <sub>50</sub> [μΜ] <sup>a</sup>	T. brucei EC <sub>50</sub> [μM] <sup>b</sup>	<i>HepG2</i> EC <sub>50</sub> [μΜ] <sup>b</sup>	SI <sup>c</sup>
7	-+-	95	7.2 (6.5–7.9)	>100	>13.8
14	-+-	>1000	32 (27–37)	>100	>3.1
15	-t-	>1000	>100	>100	-
16	OH	273	5.3 (4.8–5.8)	>100	>18.9

 $<sup>^{\</sup>rm a}$  EC  $_{\rm 50}$  values were calculated as a Hill curve fit to 12-point titration (n = 4), with SD mostly within 20 %.

 $<sup>^</sup>b$  EC  $_{\!\!50}$  values are shown as mean (n = 4). Values in parentheses are 95 % confidence intervals.

<sup>&</sup>lt;sup>c</sup> The selectivity index is calculated as HepG2 EC<sub>50</sub>/T. brucei EC<sub>50</sub>.

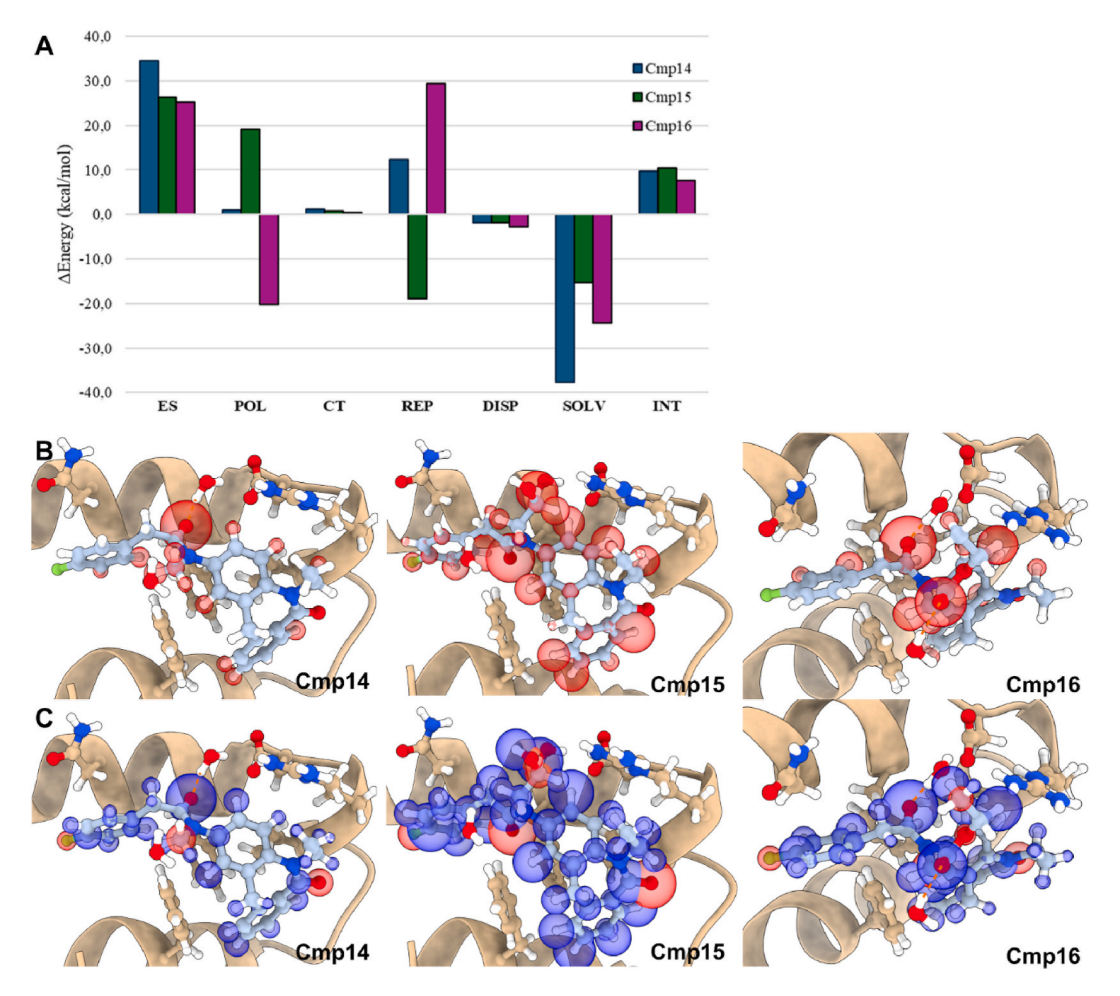


Fig. 6. The QM-EDDAs for the interactions of compounds 14–16 with *Tb*PEX14. A) Differences in the interaction contributions of analogs 14–16 with *Tb*PEX14, with respect to compound 7. B) The REP maps for binding modes of compounds 14 (first), 15 (second) and 16 (last) to *Tb*PEX14. The number of interaction points and their strength seem larger for compound 15. This is an artefact of the representation, as the atomic contribution for each EDDA term is normalized to the strongest interaction recorded for each molecule. C) The INT maps for binding modes of compounds 14 (first), 15 (second) and 16 (last) to *Tb*PEX14. Only the maps showing the most important contributions are shown here. All maps for compounds 14–16 are provided in Supplementary Data B (Fig. S3B–D).

Consequently, if ligand-protein interactions are drastically weakened, this may lead to a pattern where all signals are more intense despite no significant changes in the binding pose. Such an illustration artefact is observed for compound 15, its binding mode analysis, and all the respective maps (Fig. 6B and C). This is also reflected in a lower electronic repulsion contribution for the binding of compound 15 to PEX14 with respect to the interactions with compounds 7, 14, and 16. This indicates a decrease in the protein-ligand interaction surface. Overall, the binding pose of this inhibitor shows a significant deterioration of electrostatics and polarization interactions. Despite the larger surface area of compound 15 compared to other derivatives discussed, the ligand-protein interaction surface is negatively affected because of the unfavorable positioning of the exocyclic amide group on the protein surface. Finally, the solvation contributions indicate that, compared to compound 7, analog 15 is better stabilized in an aqueous solution than in the protein pocket (Fig. 6A). This is seen in the respective EDDA plots and is most likely caused by an inadequate binding pose.

We then set out to rationalize the observation that the ethox-ycarbonylmethyl analog **16** disrupts the PEX5-*Tb*PEX14 PPI, albeit two-fold weaker than compound **7**. This seemed counterintuitive, especially given the computational results for the structurally similar, inactive

alcohol 15. However, the docking pose of compound 16 shows the capability of the carbonyl oxygen of its ester moiety to form a hydrogen bond with one of the explicit solvation waters preserved in our docking protocol. At the same time, the other water molecule is H-bonded by the exocyclic carbonyl oxygen. Both these interactions can be followed in the total interaction maps (Fig. 6C). The electronic repulsion maps can explain the lower affinity of derivative 16 compared to the parent compound 7. The latter show that, to establish the hydrogen bond between the carboxylic ester and the solvation water, the methylene linker to the carboxamide must be oriented near the solvation water. The total interaction maps (Fig. 6C-III) show that this interaction is repulsive and destabilizes the ligand-protein complex. The above effects are reflected in the respective energy contributions in the column plot. Although compound 16 can form hydrogen bonds with two solvation waters, these interactions are weaker than in compound 7 because of the destabilizing electrostatic contributions.

# 2.3.2. SAR of the substituents in the benzylic position

The available structures of *Tb*PEX14 show the presence of hydrophilic N13 and K38 side chains opposing each other at the rim of the Trp hotspot. Thus, another set of compounds, **17–26**, was prepared to

**Table 4** SAR of the substituents in the benzylic position.

#	R	<i>Tb</i> PEX14 EC <sub>50</sub> [μM] <sup>a</sup>	T. brucei EC <sub>50</sub> [μM] <sup>b</sup>	$HepG2 \ EC_{50} \ [\mu M]^b$	SI <sup>c</sup>
7	× <sub>N</sub>	94	7.2 (6.5–7.9)	>100	>13.8
17	× <sub>N</sub> ö <sub>h</sub>	167	13 (11–15)	>100	>7.7
18	×N D O O O O O O O O O O O O O O O O O O	156	14 (12–16)	>100	>7.1
19	N N N N N N N N N N N N N N N N N N N	152	16 (13–17)	>100	>6.2
20	× NH OH	337	57 (49–66)	>100	>1.8
21	N O OCOCH3	303	12 (10–15)	15 (10–21)	1.2
22	NH COOH	334	>100	>100	-
23	N COOE	348	14 (13–15)	>100	>7.1
24	× <sub>N</sub>	>1000	31 (28–33)	>100	>3.2
25	× <sub>N</sub> Nih	361	33 (22–47)	>100	>3.3
26	×H	79	6.0 (5.0-6.9)	>100	>16.7

 $<sup>^{\</sup>rm a}$  EC<sub>50</sub> values were calculated as a Hill curve fit to 12-point titration (n = 4), with SD mostly within 20 %.

address these amino acids by installing various polar residues at the benzylic position of the arylacetamide moiety (Table 4). The mandelate derivative 17, its acetoxy-analog 18, and the formamide 19 were designed to provide polar interactions with the N13 residue or interact with the solvation waters while maintaining a low-energy ligand conformation. To our disappointment, these compounds provided lower levels of PEX5-TbPEX14 PPI inhibition compared to 7 (EC $_{50} = 167 \, \mu M$ , 156  $\mu M$  and 152  $\mu M$ , respectively). The respective -CH $_{2}$ - homologs of 17 and 18, derivatives 20 and 21, were roughly twice less potent (EC $_{50} = 337 \, \mu M$  and 303  $\mu M$ , respectively) as compound 7, just as the carboxylic acid 22 and carboxylate ester 23 (EC $_{50} = 334 \, \mu M$  and 348  $\mu M$ , respectively). We have also attempted to improve the activity of 17 and 19 by reducing the number of rotatable bonds. To this end, we synthesized the respective oxazolidine-2,4-dione 24 and imidazolidine-2,4-dione 25

derivatives. These modifications did not lead to an enhancement of the compounds' activity over the parent molecules. Compound 24 did not disrupt the PEX5-TbPEX14 PPI at concentrations up to 1 mM, whereas derivative 25 was roughly twice less potent as the parent  $19~({\rm EC}_{50}=361~\mu{\rm M})$ . The last compound from this series was obtained by transforming the benzylic -CH2- to a carbonyl group in the benzylic position. The resulting phenylglyoxylate 26 was twice as potent in disrupting the PEX5-TbPEX14 PPI as its –OH analog 17 and slightly more active than compound 7 (EC50 $=79~\mu{\rm M})$ . The distance between the inserted carbonyl oxygen of the compound and the hydrophilic protein appears too large for forming contacts with protein residues. Therefore, it is more likely that it contributes to the formation of a more favorable water network.

 $<sup>^{</sup>b}$  EC $_{50}$  values are shown as mean (n = 4). Values in parentheses are 95 % confidence intervals.

 $<sup>^{\</sup>rm c}\,$  The selectivity index is calculated as HepG2 EC50/T. brucei EC50.

**Table 5** SAR of the MCR scaffolds.

#	R	<i>Tb</i> PEX14 EC <sub>50</sub> [μM] <sup>a</sup>	T. brucei EC <sub>50</sub> [μM] <sup>b</sup>	<i>HepG2</i> EC <sub>50</sub> [μM] <sup>b</sup>	SI <sup>c</sup>	#	R	TbPEX14 EC <sub>50</sub> [μM] <sup>a</sup>	T. brucei EC <sub>50</sub> [μM] <sup>b</sup>	<i>HepG2</i> EC <sub>50</sub> [μΜ] <sup>b</sup>	SI <sup>c</sup>
27	OH	409	16 (15–17)	58 (51–66)	3.6	36	СООН	158	27 (23–30)	>100	>3.7
28	P(O)(OCH <sub>3</sub> ) <sub>2</sub>	247	6.4 (5.6–7.2)	59 (45–77)	9.2	37	P(O)(OCH <sub>3</sub> ) <sub>2</sub>	29	10 (8–12)	50 (42–57)	5.0
29	P(O)(OCH <sub>3</sub> ) <sub>2</sub>	85	7.0 (5.8–8.3)	>100	14.3	38	P(O)(OCH <sub>3</sub> ) <sub>2</sub>	28	8.6 (7.2–10.1)	6.3 (5.8–6.8)	<1.0
30	P(O)(OCH <sub>3</sub> ) <sub>2</sub>	237	43 (38–48)	>100	>2.3	39	P(O)(OCH <sub>3</sub> ) <sub>2</sub>	24	7.2 (6.3–8.1)	16 (14–17)	2.2
31	P(O)(OCH <sub>3</sub> ) <sub>2</sub>	158	5.2 (4.6–5.9)	40 (34–48)	7.7	40	P(O)(OCH <sub>3</sub> ) <sub>2</sub>	70	3.3 (3.0–3.6)	10 (9–11)	3.0
32	CONHCH₂COOE HN	144	3.4 (3.1–3.7)	>100	>29.4	41	P(O)(OCH <sub>3</sub> ) <sub>2</sub>	112	3.1 (2.9–3.3)	14 (12–16)	4.5
33	P(O)(OCH <sub>3</sub> ) <sub>2</sub>	>1000	>100	>100	-	42	CONHCH <sub>2</sub> COOEt	178	3.7 (3.5–4.0)	>100	>27.0
34	OH	116	25 (21–29)	28 (19–40)	1.1	43		>1000	3.6 (3.3–3.9)	18 (16–21)	5.0
35	OH	98	12 (9–14)	58 (43–68)	4.8						

 $<sup>^{</sup>a}$  EC50 values were calculated as a Hill curve fit to 12-point titration (n = 4), with SD mostly within 20 %.

# 2.3.3. SAR of the MCR scaffolds

Our other design strategy took advantage of the fact that the exocyclic aniline may serve as a convenient exit vector for the derivatization of the dibenzo[b,e]azepin-6(6H)-one inhibitors by multicomponent reaction (MCR) chemistry. Some MCRs have been known to be very useful in drug discovery since they can deliver drug-like compounds with unique structures using a relatively straightforward chemistry [29]. Here, we utilized Petasis, Ugi, and Kabachnik-Fields MCRs, which constitute powerful tools to implement various amino acid, amino alcohol, amino amide and amino phosphonate scaffolds in a one-pot condensation of simple reagents. Particularly, we employed these MCRs to decorate the aniline with residues, in which various arvl and arylalkenyl moieties addressing the lipophilic Trp pocket were attached to the same carbon atom as the polar hydroxymethyl, carboxylate, carboxamide or phosphonate groups pointing towards the hydrophilic amino acid side chains present in the vicinity of this hotspot (Table 5).

The previously investigated compounds 7-25 addressed the Trp pocket of TbPEX14 with a single benzene ring delivered into this hydrophobic cavity via an acetamide linker (Tables 1-4). We have shown here and in our previous reports (Fig. 3B) [22,25,28] that such positioning of the benzene ring aligns well with the native binding of PEX5 tryptophan side chain to the PEX14 Trp pocket and that it can result in potent PEX5-PEX14 PPI inhibitors. However, we were also interested in seeing whether we could address this pocket with biaromatic ring systems, just as it is observed in the structure of the PEX5-PEX14 PPI (Fig. 1A). To this end, we obtained the MCR products 27, and 29 with either benzofuran or indole moieties attached to the quaternary carbon atom, which links them to the aniline nitrogen (Table 5). The benzofuran-containing Petasis product 27 displayed only weak activity in disrupting the PEX5-PEX14 PPI (EC<sub>50</sub> = 409  $\mu$ M), while its phosphonate analog 28, derived from the Kabachnik-Fields reaction, was roughly twice as potent (EC<sub>50</sub> = 247  $\mu$ M). Propitiously, the indole analog **29** of benzofuran **28** conferred a further gain in activity (EC<sub>50</sub> =  $85 \mu M$ ).

 $<sup>^{\</sup>rm b}$  EC<sub>50</sub> values are shown as mean (n = 4). Values in parentheses are 95 % confidence intervals.

<sup>&</sup>lt;sup>c</sup> The selectivity index is calculated as HepG2 EC<sub>50</sub>/T. brucei EC<sub>50</sub>.

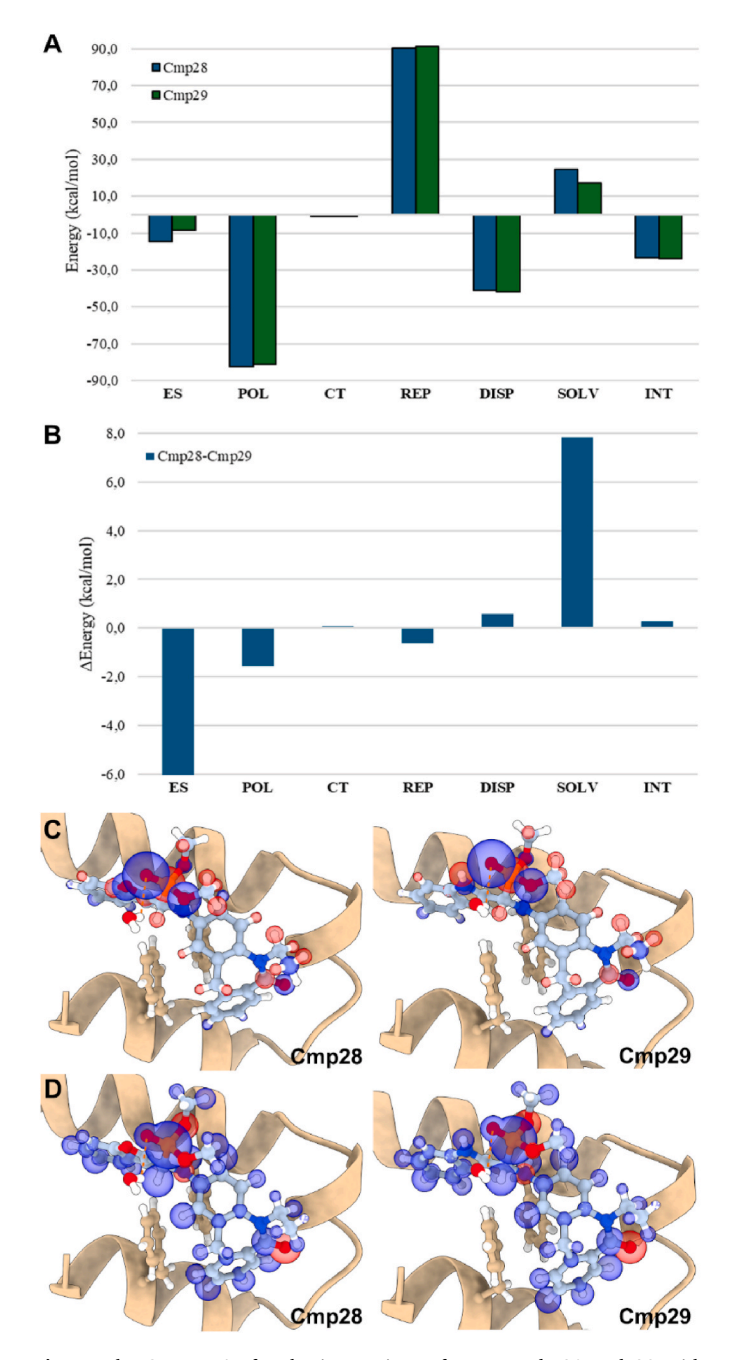


**Fig. 7.** The QM-EDDAs for the interactions of compounds **28** and **29** with *Tb*PEX14. A) The respective EDDA results for compounds **28** and **29**. B) The relative EDDA of compounds **28** and **29** shows the fine differences in binding contributions. C) The ES maps for binding modes of compounds **28** (left) and **29** (right) to *Tb*PEX14. D) The INT maps for binding modes of compounds **28** (left) and **29** (right) to *Tb*PEX14. Only the maps showing the most important contributions are shown here. All maps for compounds **28** and **29** are provided in Supplementary Data B (Figures SB-D).

Interestingly, the QM-EDDA calculations (Fig. 7, S4A-F, Table S4) indicated that, although the benzofuran oxygen atom in compound **28** provides an electrostatic stabilization of the inhibitor-protein complex, this effect is cancelled out in the total interaction maps (Fig. 7B and D). This is reflected in the neutral contribution of this oxygen to the ligand-protein interaction energy, resulting from the cancellation of favorable electrostatics by the solvation effects (Fig. 7A and D). We attribute this to electrostatic shielding from the protein environment in which the ligand is embedded and to the benzofuran oxygen weak hydrogen bond acceptor character (Fig. S4E). On the contrary, the

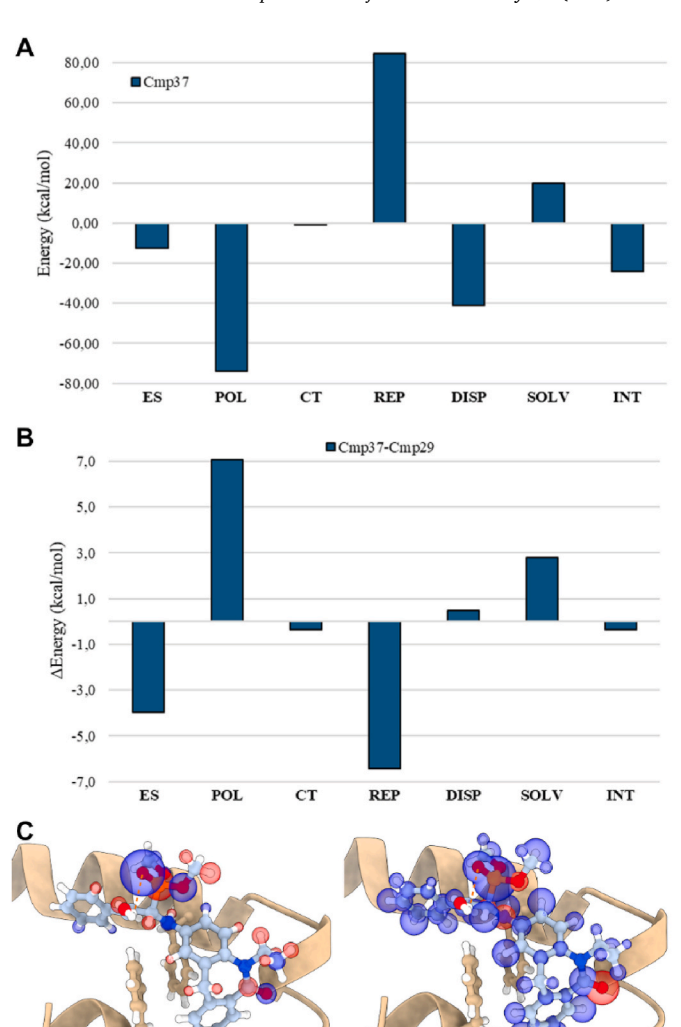


**Fig. 8.** The QM-EDDA for the interactions of compound **37** with *Tb*PEX14. A) The EDDA results for compound **37**. B) The relative EDDA of compounds **37** and **29**, showing the differences in binding contributions. C) The ES (left) and the INT (right) maps of compound **37**. Only the maps showing the most important contributions are shown here. All maps for compound **37** are provided in Supplementary Data B (Fig. S4B–D).

Cmp37

contribution from the indole NH group in compound 29 remains favorable in the INT maps (Fig. 7D). Similar to compound 28, there is an interplay between electrostatics and solvation. However, the solvent stabilization by the indole ring in the protein pocket is favorable in the case of analog 29. This is because the indole NH is a better hydrogen bond donor than the benzofuran oxygen is an acceptor (Fig. S4E). The EDDA calculations also show the significant contributions of the phosphonate groups for binding ligands 28 and 29 to *Tb*PEX14. First, the oxygen atoms of these functional groups form hydrogen bonds with the important solvation waters, which makes them the main electrostatic anchors of the ligands to the protein. Interestingly, the phosphorous atom also provides a significant energetic contribution (Fig. 7D). This atom primarily affects the solvation and polarization stabilization. Still, it also supplies and supports the electrostatic interactions of the oxygen atoms of the phosphonate group by donating its electronic density.

Other indole derivatives obtained, the C-3 regioisomer **30** and the 5-fluoro derivative **31**, were markedly weaker than the parent compound **29** (EC<sub>50</sub> = 238  $\mu$ M and 157  $\mu$ M, respectively). Similar results were recorded for the Ugi product **32** (EC<sub>50</sub> = 144  $\mu$ M). To further highlight the importance of the presence of the diaromatic system in this series of PEX5-PEX14 PPI inhibitors, we have synthesized a monoaromatic ring

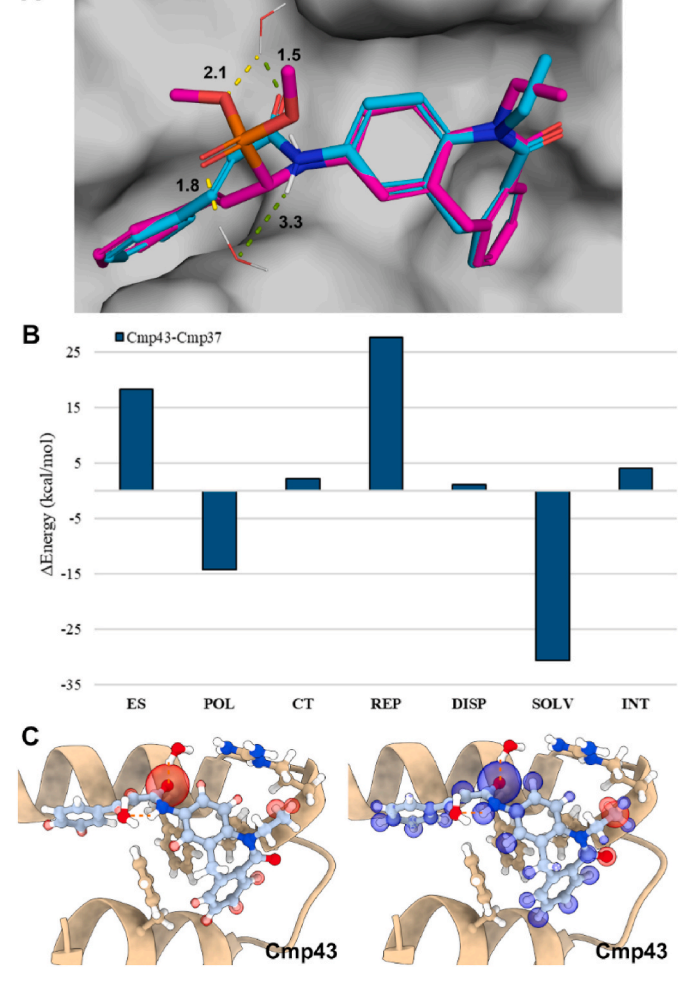


**Fig. 9.** The QM-EDDA for the interactions of compounds **43** with *Tb*PEX14 NTD. A) Comparison of the binding poses of compounds **37** (magenta) and **43** (blue) to *Tb*PEX14 NTD. Important hydrogen bonds are marked with the solvation waters (yellow and green, for compounds **37** and **43**, respectively). The distances between the respective hydrogen bond donors and acceptors are given in Å. B) The relative EDDA of compounds **43** and **37**, showing the differences in binding contributions. C) The REP (left) and the INT (right) maps of compound **43**. Only the maps showing the most important contributions are shown here. All maps for compound **43** are provided in Supplementary Data B (Fig. S5). (For interpretation of the references to color in this figure legend, the reader is referred to the Web version of this article.)

derivative **33** of inhibitor **29**. This control compound was inactive at concentrations up to 1 mM, most likely due to its inability to efficiently fill the Trp pocket.

Another subset of compounds, the vinylbenzene derivatives **34–43**, was designed to preserve a general atomic distribution and the shape of the benzofuran and indole systems, while achieving partial conformational flexibility by deleting the bridging heteroatom (Table 5). Propitiously, a vinylbenzene derivative **34** derived from Petasis MCR displayed an almost 4-fold gain in the potency of inhibiting the PEX5-TbPEX14 PPI (EC $_{50}=116~\mu M$ ), when compared to the parent benzofuran **27**. Other Petasis products, the bis(hydroxymethyl) **35** and carboxylate **36** derivatives, did not confer further affinity enhancement, displaying comparable activity to compound **34** (EC $_{50}=88~\mu M$  and 158  $\mu M$ , respectively). We observed a remarkable improvement within the phosphonate series, with almost an order of magnitude gain of activity of vinylbenzene **37** (EC $_{50}=29~\mu M$ ) with respect to its benzofuran analog **28** and a three-fold increase in potency compared to its indole counterpart **29**. To rationalize the beneficial effect of transitioning from

condensed aromatic ring systems to vinylbenzene, we compared the QM-EDDA results for the ligand-protein complexes of compounds 28 and 29 with those obtained for 37 (Fig. 8). We observed an excellent correlation between the activity of those compounds in the AlphaScreen assay and the theoretical calculations (Fig. S4A). A thorough analysis of the computational results indicated slight differences between the binding poses of the biaromatic and vinylbenzene ligands and confirmed the expected gain in flexibility of the latter in the Trp pocket of *Tb*PEX14. Consequently, the vinylbenzene group of compound 37 can reach slightly deeper into this cavity (Fig. S4F). This translates into optimized interactions, as seen in the decomposed energy values and the corresponding maps (Table S4 and Fig. 8, S4B-D). The electrostatic interactions with the protein are closer to those observed in compound 28, while the solvation destabilization is similar to that recorded for compound 29 (Table S4). Although compound 37 has fewer atoms than compounds 28 and 29, which is reflected in the repulsion and polarization contributions (Fig. 8B), it offers dispersion interactions with the protein resembling those of the other two ligands (Table S4). Overall, compound 37 can be seen as taking advantage of the best features of 28 and 29. We have also conducted a preliminary analysis of the influence of phenyl substitution pattern in 37. Here, we observed that para-F and Me substituents are tolerated, albeit the respective 38 and 39 derivatives did not confer superior activity than the parent compound ( $EC_{50} = 28$  $\mu M$  and 25  $\mu M$ , respectively). Besides this, the meta-F and Me counterparts 40 and 41 (EC<sub>50</sub> = 70  $\mu M$  and 112  $\mu M$ , respectively) were less potent in inhibiting the PEX5-TbPEX14 PPI. We have also synthesized compound 42, a vinylbenzene analog of the indole derivative 32. This compound did not confer improvement in activity.

Finally, to verify whether the introduction of the vinylbenzene would also benefit the carboxamide series, we synthesized compound **43**, a carboxamide analog of the MCR product **37**. Interestingly, this derivative showed a complete lack of PEX5-*Tb*PEX14 PPI inhibition. The docking poses of compounds **43** and **37** are conserved regarding the arrangements of their tricyclic cores on the *Tb*PEX14 surface and the positions of the benzene rings in the Trp hotspot (Fig. 9A). However, they differ in the arrangements of the moieties projecting the benzene rings into the Trp pocket. Although the carboxamide group of compound **43** forms important interactions with the two solvation waters, the overall positioning of this acrylamide fragment should be less favorable, according to the AlphaScreen data.

To best understand the effects leading to the loss of activity of compound 43, we ran EDDA calculations for its complex with TbPEX14 and compared the results with those obtained for analog 37 (Fig. 9BC, S5 and Table 5). The computations show a 4.1 kcal/mol difference in the binding energies of these compounds (Tables S4 and S5). Although EDDA disregards entropic contributions, this high value accurately reflects the loss of experimentally evaluated activity of compound 43. A closer look at the total interaction maps (Fig. 9C) reveals a strong interaction of the exocyclic amide oxygen in 43 with the solvation water over a distance of approximately 1.5 Å. On the other hand, the distance between the hydrogen bond of the NH proton of this same amide group and the second water molecule is larger than 3.3 Å, which results in a much weaker interaction. On the contrary, the phosphonate group in compound 37 projects hydrogen bond-forming atoms at more suitable distances from the solvation water molecules (1.8 and 2.1 Å). This ensures a more balanced binding mode, where two equally strong hydrogen bonds are formed instead of only one. Further, the binding mode of compound 37 places less strain on other ligand atoms in the proximity of the phosphonate functional group. We reason that the imbalance in the interaction pattern of compound 43 with the neighboring water leads to slight deviations in the binding mode of this ligand to TbPEX14. This, together with the very close distance between the exocyclic amide oxygen and the solvation water molecule, is reflected by an almost 30 kcal/mol increase in electronic density repulsion (Fig. 9B). This effect alone justifies the dominance of the interaction between the amide oxygen atom and the solvation water in the total interaction maps

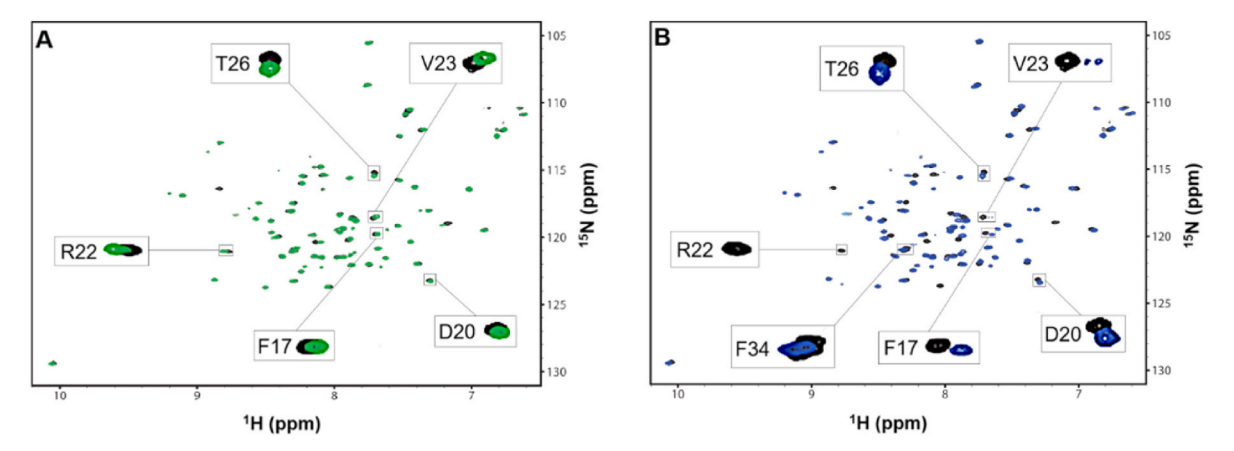


Fig. 10. Evaluation of binding of compounds 7 and 37 to TbPEX14 NTD by  $^{1}H_{-}^{15}N$  heteronuclear single quantum coherence (HSQC) NMR spectroscopy. A)  $^{1}H_{-}^{15}N$  HSQC spectrum of 200 μM  $^{2}H_{-}^{15}N$  HSQC spectrum of 200

(Fig. 9C). Differences between other EDDA binding contributions of compounds **43** and **37** to *Tb*PEX14 are affected by how the benzene functional groups of these analogs are projected into the Trp hotspot of TbPEX14. Here, we see a steep increase in electrostatics, reflecting the weakening of an important interaction with one of the solvation waters and a strong solvation stabilization. The latter reflects a less polar ligand

surface area for compound **43**, which is, in this case, better stabilized in the PEX5-*Tb*PEX14 PPI interface. Overall, the calculations performed on the docked poses of compounds **37** and **43** rationalize their relative affinities to *Tb*PEX14 mostly by the capabilities of each molecule to effectively capture the water-mediated interactions with the protein.

Scheme 1. i. SOCl<sub>2</sub>, MeOH, 92 %; ii.1. o-Fluoronitrobenzene, NaH, DMF; 2.  $HCl_{aq}$ ; 79 %; iii.1. NaOH<sub>aq</sub>, 1,4-dioxane; 2.  $HCl_{aq}$ ; iv.1.  $K_2CO_3$ , DMF; 2.  $HCl_{aq}$ ; (iii-iv:70 %); v. Fe, AcOH; 97 %; vi. HNO<sub>3</sub>, AcOH; 57 %; vii. SnCl<sub>2</sub>, EtOH; quant.; viii.1. EtBr, NaH, DMF; 2.  $NH_4Cl$ ; 99 %; ix. ix.

 $\begin{array}{l} \textbf{Scheme 2.} \ i. \ p-FC_6H_4CH_2CO_2H, \ EDC\cdot HCl, \ Et_3N, \ DMAP, \ DCM; \ 77\% \ (from \ \textbf{44}); \ \emph{ii.} \ p-FC_6H_4CH_2CO_2H, \ EDC\cdot HCl, \ Et_3N, \ DMAP, \ DCM; \ 81\% \ (from \ \textbf{45}); \ \emph{iii.} \ MeI, \ K_2CO_3, \ DMF; \ 45\%; \ \emph{iv.} \ \emph{i-PrBr}, \ KI, \ TBAB, \ K_2CO_3, \ DMF; \ 60\%; \ \emph{v.} \ BrCH_2CO_2Et, \ Cs_2CO_3, \ DMF; \ 71\%; \ \emph{vi.} \ MeI, \ 50\% \ NaOH_{aq}, \ TBAB, \ 1,4-dioxane; \ 59\% \ (from \ \textbf{7}). \end{array}$ 

Scheme 3. i. p-FC<sub>6</sub>H<sub>4</sub>CH<sub>2</sub>CO<sub>2</sub>H, EDC·HCl, DMAP, DCM; 85 %.

# 2.4. NMR validation experiment

Fig. 4 shows the capability of our in silico protocol to accurately predict the binding pose of carboxamide derivative 7 to PEX14, which was nearly identical to that of analog 5 in its cocrystal with the protein. Further, the AlphaScreen assay results show disruption of the PEX5-TbPEX14 PPI by the synthesized compounds, and that the magnitude of this activity can be correlated with the respective EDDA results. To obtain further experimental proof that the PEX5-TbPEX14 PPI inhibition is a direct result of the reversible binding of the compounds to TbPEX14 NTD, we performed <sup>1</sup>H, <sup>15</sup>N 2D heteronuclear single-quantum coherence correlation NMR experiments (Fig. 10). For this assay, we selected compounds 7 and 37, as they not only significantly differ in their AlphaScreen activity but also display quite pronounced differences in their chemical structures. The results show that in both cases, the application of a compound causes changes in the chemical shifts of the NMR signal resonances of the protein, confirming binding. Further, compound 7 interacts with TbPEX14 NTD in fast exchange binding kinetics on the NMR chemical shift time scale (Fig. 10A), whereas compound 37 causes more significant changes in the NMR spectra (most peaks show larger chemical shift perturbations and some, i.e., V23 and R22 disappear from the spectrum, indicating intermediate exchange, Fig. 10B). This likely reflects its higher affinity for *Tb*PEX14 NTD and follows the activity trend observed in the AlphaScreen assays. Importantly, both NMR experiments show that affected resonances of the *Tb*PEX14 NTD spectrum can be attributed to residues in proximity to the binding site for the PEX5 WxxxF motif. This indicates that compounds 7 and 37 bind the protein at the expected binding site based on the *in silico* experiments.

# 2.5. Cellular activity of tricyclic PEX5-TbPEX14 PPI inhibitors

We also determined whether the investigated compounds exhibit *in vitro* cellular activity. We tested all inhibitors against T. b. brucei bloodstream from protists as model organisms, relying on peroxisomal import of important cytosolic enzymes. We determined the TbPEX14 ligand cytotoxicity in HepG2 cells (Tables 1–5). The compounds displayed varied levels of trypanocidal activities, some having low-micromolar  $IC_{50}$  values, comparable to those observed for some PEX5-TbPEX14 PPI inhibitors previously studied. [22–24,28]. In line with our previous findings, the  $EC_{50}$  values of the compounds for the cell-based activities ( $EC_{50}$ ) are lower than the ones for the PEX5-TbPEX14 PPI inhibition. This results from disrupting the PEX5-TbPEX14 complex formation, which impairs the compartmentation of glycolytic enzymes inside glycosomes. These enzymes lack feedback regulation; thus, their

Scheme 4. *i.* BrCH<sub>2</sub>CO<sub>2</sub>Et, AcONa, EtOH; 42 %; *ii.* (HOCHCH<sub>2</sub>O)<sub>2</sub>, AcOH, Na<sub>2</sub>SO<sub>4</sub>, THF; then NaBH(OAc)<sub>3</sub>; 84 %; *iii. p*-FC<sub>6</sub>H<sub>4</sub>CH<sub>2</sub>CO<sub>2</sub>H, EDC·HCl, DCM; 55 % (from 58); *iv.* 1. *p*-FC<sub>6</sub>H<sub>4</sub>CH<sub>2</sub>CO<sub>2</sub>H, EDC·HCl, Et<sub>3</sub>N, DMAP, DCM; 2. NaOH<sub>aq</sub>, 1,4-dioxane, 12 % (from 59, over 2 steps).

Scheme 5. i. 1. LDA, THF; 2. BrCH<sub>2</sub>CO<sub>2</sub>Et; 3. HCl<sub>aq</sub>; 22 %; ii. EDC·HCl, DCM; 84 % (from **60**); iii. EDC·HCl, DCM; 83 % (from **61**); iv. 1 NaOH<sub>aq</sub>, 1,4-dioxane, then 2 HCl<sub>aq</sub>; 89 % (from **23**); v. K<sub>2</sub>CO<sub>3</sub>, MeOH; 77 % (from **21**).

Scheme 6. i. Ac<sub>2</sub>O, HCO<sub>2</sub>H, 70 %; ii. EDC·HCl, Et<sub>3</sub>N, DMAP, DCM; 40 % (from 63), iii. EDC·HCl, Et<sub>3</sub>N, DMAP, DCM; 60 % (from 64); iv. HCl<sub>aq</sub> 1,4-dioxane, quant., from 19); v. K<sub>2</sub>CO<sub>3</sub>, MeOH; 96 % (from 18); vi. CDI, 1,4-dioxane, 43 % (from 65), vii. CDI, 1,4-dioxane, 94 % (from 17).

Scheme 7. i. PhC(O)CO<sub>2</sub>H, EDC·HCl, NEt<sub>3</sub>, DMAP, DCM; 59 %.

mislocalization to the cytosol leads to unregulated glucose phosphory-lation and ATP depletion, therefore amplifying toxicity [20]. However, the current study cannot exclude the occurrence of additional off-target effects, especially since several compounds show poor correlation of the trypanocidal activity and the PPI inhibition. In addition, permeability differences between the respective derivatives may exist, which further complicates the analysis of the cellular assays results. Most inhibitors displayed selectivity between their trypanocidal activity and cytotoxicity against HepG2 cells. Some compounds killed the parasites at low micromolar concentrations without showing HepG2 cytotoxicity at  $50{\text -}100~\mu\text{M}$  concentrations.

# 2.6. Chemistry

Target PEX5-PEX14 PPI inhibitors 7-43 were synthesized as shown

**Scheme 10.** *i.* Indole-2-CHO, CNCH<sub>2</sub>CO<sub>2</sub>Et. PhP(O)H(OH), MeOH; 44 %; *ii.* (*E*)-PhCH=CHCHO, CNCH<sub>2</sub>CO<sub>2</sub>Et, PhP(O)H(OH), EtOH; 23 %.

Scheme 11. i.1. PhCH=CHCO<sub>2</sub>H (E), EDC·HCl, DCM.

Scheme 8. *i*. Benzofuran-2-B(OH)<sub>2</sub>; (HOCHCH<sub>2</sub>O)<sub>2</sub>, MeOH; 90 %, *ii*. PhCH=CHB(OH)<sub>2</sub> (*E*), (HOCHCH<sub>2</sub>O)<sub>2</sub>, MeOH; 44 %; *iii*. (*E*)-PhCH=CHB(OH)<sub>2</sub>, [(HOCH<sub>2</sub>)<sub>2</sub>CO]<sub>2</sub>, MeOH; 61 %; *iv*. (*E*)-PhCH=CHB(OH)<sub>2</sub>, HO<sub>2</sub>CCHO·H<sub>2</sub>O, MeOH; 83 %.

Scheme 9. *i*. Benzofuran-2-CHO,  $(MeO)_2P(O)H$ , THF; 56 %; *ii*. Indole-2-CHO,  $(MeO)_2P(O)H$ , THF, 93 %; *iii*. Indole-3-CHO,  $(MeO)_2P(O)H$ , THF; 86 %; *iv*. 5-F-indole-2-CHO,  $(MeO)_2P(O)H$ , 1,4-dioxane; 92 %; *v*. *p*-FC<sub>6</sub>H<sub>4</sub>CHO,  $(MeO)_2P(O)H$ , THF; 81 %; *vi*. *p*-FC<sub>6</sub>H<sub>4</sub>CH=CHCHO (*E*),  $(MeO)_2P(O)H$ , THF; 79 %; *vii*. PhCH=CHCHO (*E*),  $(MeO)_2P(O)H$ , THF; 59 %; *viii*. *p*-MeC<sub>6</sub>H<sub>4</sub>CH=CHCHO (*E*),  $(MeO)_2P(O)H$ , THF; 91 %; *ix*. *m*-FC<sub>6</sub>H<sub>4</sub>CH=CHCHO (*E*),  $(MeO)_2P(O)H$ , THF; 66 %; *x*. *m*-MeC<sub>6</sub>H<sub>4</sub>CH=CHCHO (*E*),  $(MeO)_2P(O)H$ , THF; 81 %.

Scheme 12. i. MeI, TBAB, K<sub>2</sub>CO<sub>3</sub>, DMF; 59 %; ii. H<sub>2</sub>SO<sub>4</sub>, MeOH; 98 %; iii. Cs<sub>2</sub>CO<sub>3</sub>, DMF; 38 %; iv. 1. NaOH<sub>aq</sub>, 1,4-dioxane, 2. AcOH; v. Fe, AcOH; 98 % (overall iv-v); vi. HNO<sub>3</sub>, H<sub>2</sub>SO<sub>4</sub>; 71 %; vii. EtBr, K<sub>2</sub>CO<sub>3</sub>, DMF; 66 %; viii. SnCl<sub>2</sub>, EtOH; 76 %; ix. p-FC<sub>6</sub>H<sub>4</sub>CH<sub>2</sub>CO<sub>2</sub>H, EDC·HCl, Et<sub>3</sub>N, DMAP, DCM; 96 %.

in Schemes 1–12. The key intermediates 44, 45, and 46 for compounds 7, 9-43 were obtained by adopting a synthetic strategy employing a literature tandem nitro group reduction/intramolecular cyclization (lactamisation) leading to the key tricyclic 5,11-dihydro-6*H*-dibenzo[*b*, e]azepin-6-one scaffold [30], as shown in Scheme 1. Homo-phthalic acid 47 was diesterified [31] with MeOH in a process catalyzed by HCl generated in situ from the reaction of SOCl<sub>2</sub> with MeOH. Subsequently, the obtained diester 48 was deprotonated with NaH, and the in situ formed carbanion was subjected to nucleophilic aromatic substitution with o-fluoronitrobenzene. The resulting product 49 was hydrolyzed [32] to diacid 50. Subsequently, decarboxylation of 50 was performed, which was facilitated by the presence of the o-nitro group stabilizing the formation of the intermediary benzylic-type carbanion, as previously described [33]. The obtained intermediate 51 was reduced with Fe/AcOH to aniline **52**, which underwent a spontaneous cyclization [30] to 5, 11-dihydro-6H-dibenzo[b,e]azepin-6-one 53. A regioselective mononitration of 53, followed by the reduction of the resulting nitroarene 54 with SnCl<sub>2</sub>/EtOH, gave aniline 44, which served as a key intermediate in the synthesis of final compound 9. Intermediate 45 for the synthesis of inhibitors 7,14-43 was obtained by deprotonation and N-ethylation of lactam 53, followed by a regioselective mononitration of the resulting 55 and reduction of the nitro group in 56. Alternatively, 56 was obtained employing a reversed sequence with the N-alkylation of the nitro-lactam 54 in a first step, followed by the reduction of the resulting **56.** The advantage of this altered synthetic protocol is the use of milder deprotonation conditions (using carbonates in the presence of tetrabutyl ammonium bromide (TBAB)), as the presence of the nitro group in the p-position stabilizes the ambident amidate. This reaction proceeded with the formation of considerable amounts of O-ethylated 11H-dibenzo[b,e] azepine byproduct 57, which was subsequently reduced to intermediate 46 used for the synthesis of inhibitor 13.

The target compounds **7**, **9–12**, having various substituents attached to the lactam moiety, were obtained from the respective intermediates **44**, **45** and **47**, as shown in Schemes 2 and 3. The respective carbodiimide/DMAP-mediated amidation reactions with p-fluorophenylacetic gave compounds **9**, **7** and **13**. The N–H proton of the

lactam moiety of tricyclic intermediate 9 is slightly more acidic than the one in the exocyclic anilide group. Therefore, the compound could be selectively deprotonated with carbonates and N-alkylated with MeI, i-PrBr (in the presence of TBAB) or BrCH $_2$ CO $_2$ Et to give the respective inhibitors 10–12.

The analogs 14–16 of compound 7 with various alkyl groups in the exocyclic amide nitrogen were synthesized as shown in Schemes 2 (compound 14) and 4 (16 and 15) The exocyclic anilide moiety in 7 was directly deprotonated using a strong base and *N*-methylated in the presence of TBAB to give tertiary amide 14. In the synthesis of other *N*-alkylated *exo*-amide derivatives 15 and 16, the alkyl moieties were introduced before the *N*-amidation reaction, as shown in Scheme 4. Alkylation of 53 with BrCH<sub>2</sub>CO<sub>2</sub>Et gave intermediate 58, whereas the reductive amination of the aniline using glycolaldehyde dimer provided 59. The subsequent EDC·HCl-mediated amidation of 58 with *p*-fluorophenylacetic acid gave the respective tertiary amide 16. The same acylation conditions applied to compound 59 resulted in simultaneous acylation of the amine and alcohol groups. Hence, an additional ester hydrolysis step was required to obtain inhibitor 15.

Target derivatives 17–23 and 24–26 with various substituents attached to the benzyl position of the p-fluorophenylacetamide moiety were synthesized as shown in Schemes 5–7. The hydroxymethyl and acetate derivatives 20–23 (Scheme 5) were synthesized by amidation reactions of 45 with the respective p-fluorophenylacetic acids 60 or 61 in the first step. Intermediate 60 was obtained from p-fluorophenylacetic acid in the Ivanov-type reaction, by C-alkylation of a dianion generated with LDA. The alternative carboxylate ester precursor 61 is commercially available. Reaction of 45 with 60 or 61 gave the corresponding esters 23 and 21, which were then subjected to basic hydrolysis or mild methanolysis, respectively, to provide carboxylate 22 and alcohol 20.

The synthesis of derivatives 17-19 and 24-25 having additional heteroatoms attached to the benzyl position of the phenylacetamide moiety is shown in Scheme 6.  $\iota$ - $\alpha$ -phenylglycine 62 was transformed into formamide 63 in an N-acylation reaction with in-situ formed acetic-formic mixed anhydride [34]. Intermediate 63 and commercially available building block 64 were used to obtain the respective inhibitors

19 and 18. The formyl and acetyl protecting groups were removed from 19 and 18 by acidic hydrolysis or methanolysis, to give the corresponding amine 65 and alcohol 17. Finally, CDI was used to cyclize amine 65 to hydantoin 25 and alcohol 17 to 2,4-oxazolidinedione 24.

The phenylglyoxalate derivative **26** was obtained using the amidation reaction of **45** with phenylglyoxylate, as shown in Scheme 7.

Inhibitors **27–42** were obtained by Petasis, Kabachnik-Fields or Ugi MCRs, as shown in Schemes 8–10. Derivatives **27,34–36** were obtained from intermediate **45** and appropriate boronic acids and carbonyl components using Petasis (boro-Mannich) MCR reaction as shown in Scheme 8.

The dimethyl amino-phosphonates **28–31,33,36–37**, and **39–41** were obtained employing Kabachnik-Fields MCR of aniline **45**, dimethylphosphite and appropriate aldehyde, as shown in Scheme 9.

Another MCR, Ugi reaction was employed in synthesizing derivatives 32 and 42, using an appropriate carboxaldehyde, ethyl isocyanoacetate and phenylphosphinic acid as an acidic activator, as shown in Scheme 10

The cinnamamide derivative **43** was obtained by acylation of **45** with cinnamic acid, as shown in Scheme 11.

Inhibitor 8 was synthesized as shown in Scheme 12. A six-step synthesis of the key tricyclic 6,11-dihydro-5*H*-pyrido[3,2-*c*] [1] benzazepin-5-one intermediate 66 was already reported in the literature [35]. However, considering our previous successful experience synthesizing an analogous 5,11-dihydro-6H-dibenzo[b,e]azepin-6-one scaffold (Scheme 1), we applied a similar approach to obtain 66. Initial attempts to synthesize the methyl ester of intermediate 67 by reacting ethyl 2-methylnicotinate with 2-fluoronitrobenzene using various bases failed. Hence, a different strategy was applied, which consisted of applying the reverse functionality of substrates. To that end, esters 68 and 69 [36] were prepared from the respective acids 70 and 71 and subjected to cross-Claisen condensation in the presence of Cs<sub>2</sub>CO<sub>3</sub>. This allowed the diester 72 to be obtained in moderate yields. Interestingly, unlike the benzene analogue 49, which required a two-step basic hydrolysis/acid treatment and additional decarboxylation (Scheme 1), the pyridine 72 underwent a smooth decarboxylation to 67 under aqueous hydrolytic conditions. The reduction of the NO2 group in compound 67, in the presence of Fe/AcOH, inspired by the literature procedure of obtaining 50 (Scheme 1) [30], gave aniline 73, which spontaneously cyclized to the key tricyclic 6,11-dihydro-5*H*-pyrido[3, 2-c] [1] benzazepin-5-one intermediate **66**. Nitration of **66** resulted in the formation of a very insoluble intermediate 74, which was selectively N-alkylated via its anion, in the presence of competitive pyridine nitrogen. This resulted in compound 75, which was subsequently reduced to aniline 76 and amidated with p-fluorophenylacetic acid to give the target inhibitor 8.

# 3. Conclusions

PPIs have long been considered a promising target class but remain challenging to target with small molecules. In our previous research, we have successfully applied structure-based drug discovery (SBDD) techniques to develop several new compound series to tackle the PEX5-PEX14 PPI. However, despite our deep understanding of the complex structural features and availability of X-ray structural data, the ligand design and the SAR rationalization remained challenging, as the experimental binding efficacy did not always match the expectations based on the structural data and docking. This manuscript combines SBDD principles with the QM-EDDA calculations to validate the central scaffold re-design strategy in a new series of PEX5-TbPEX14 PPI inhibitors. This led to novel tricyclic dibenzo[b,e]azepin-6(6H)-one TbPEX14 ligands. In addition, QM-EDDA allowed to rationalize the activities of a series of analogs of inhibitor 7, resulting from follow-up derivatization. Even without co-crystal data of the new scaffolds with the protein target, our approach yielded an overall good agreement between the QM-derived compound binding energies and the

experimental data obtained from the biophysical assays.

The employed derivatization approaches delivered diverse chemical scaffolds, including MCR products. The phenylvinyl phosphonate derivatives obtained by the Kabaschnik-Fields MCR were the most active tricyclic inhibitors of *Tb*PEX5-PEX14 PPI developed so far [28]. Thus, this moiety may constitute a new, interesting tool for targeting lipophilic PPI pockets. Some of the obtained compounds displayed trypanocidal activities. Importantly, in many cases, we observed no accompanying cytotoxicity against the HepG2 cell line.

Altogether, our results stress the potential and complementarity of the classical SBDD and QM-based approaches in a challenging area of PPI inhibitor development. Thus, the findings presented in this paper may be of a more general application in targeting PPIs and understanding the SBDD outcomes.

# 4. Materials and methods

# 4.1. Chemistry-general methods

Reagents and solvents were purchased from commercial suppliers and used without further purification. Thin layer chromatography (TLC) was carried out on Merck TLC 60 aluminium sheets (silica gel and RP-18). Normal-phase flash column chromatography (CC) was performed using Merck silica gel 60 (particle size 0.040-0.063 mm, 230-400 mesh ASTM). Reverse-phase CC separations were conducted using cartridge columns (12 g or 24g SiliCycle SiliaSep™ C18). LC-MS analyses were performed on an Agilent 1220 Infinity II Gradient LC System coupled with an Agilent LC/MSD single-quadrupole detector (column: Poroshell 120, EC-C18,  $3.0 \times 50$  mm,  $2.7 \mu m$ ; gradient: water/MeCN containing 0.1 % formic acid (v/v), 5-95 % MeCN; UV detection at 220 and 254 nm). NMR data were recorded on an Agilent 400 MHz 400-MR DD2 or a Varian NMR System (500 MHz) instrument. <sup>1</sup>H NMR peaks are reported as follows: chemical shift ( $\delta$ ) in parts per million (ppm) relative to residual non-deuterated solvent as the internal standards, multiplicity (s = singlet, d = doublet, t = triplet, q = quartet, dd = doublet of doublets, ddd = doublet of doublets of doublets, dt = doublet of triplets, m = multiplet and br = broad signal), coupling constant (in Hz), number of nuclei and proton assignment. Optical rotation analysis was performed with a PerkinElmer 241 polarimeter using a sodium lamp ( $\lambda = 589$  nm, D-line), at 20 °C. The [ $\alpha$ ]D values are reported in  $10^{-1}$  deg cm<sup>2</sup> g<sup>-1</sup>, the concentrations (c) are in g/100 mL. The final compounds were >95 % pure, as determined by NMR. The detailed synthetic protocols, compound characterization data and copies of NMR spectra are provided in Supplementary Data A.

# 4.2. In silico studies

# 4.2.1. Protein preparation

Due to the scaffold similarity, we used the high-resolution co-crystal structure of compound 5 with TcPEX14 NTD (PDB accession code: 7QRC) for in silico investigations. One of the two chains in the crystal asymmetric unit (chain B) shows a more complex water network around the ligand in the pocket and was selected for the experiments. The TbPEX14 model was built by mutation of the TcPEX14 residues near the PEX5-PEX14 PPI interface (i.e., S12 to N, Q15 to E, and N29 to S). The protein was prepared using the Protein Preparation Wizard (PPW) available from Schrödinger's Maestro [37]. Missing side chains were corrected using Prime, and the hydrogen atoms were added to the complex. The resulting structure was subsequently stripped of the co-crystallised ligand and crystallisation buffer constituents. We kept the two water molecules involved in direct hydrogen bond interactions with the ligand in all docking experiments. All other water molecules were excluded, except these two, which were retained from the initial stages of the PPW structure refinement. None of the compounds subjected to docking required special considerations regarding their protonation or tautomerization states. Therefore, we directly modified the.

sdf file containing compound 5 extracted from the PDB ID: 7QRC, added hydrogen atoms, and used the resulting structures as inputs for docking. The structural modifications of the ligands were done using Avogadro 1.2 [38].

# 4.2.2. Binding mode generation for EDDA analyses

For each compound, up to 10 binding models were generated using Glide [39]. Only the S-enantiomers of compounds 28, 29 and 37 were considered for further analysis, as their mirror images provided unreliable results, i.e., neither the generated docking poses nor the EDDA binding energies for R-enantiomers were consistent with other structural models obtained for this work. Due to the efficiency of our EDDA algorithm, we ran these calculations for all models generated by docking. We then used the EDDA binding energies to exclude structural models with too unfavorable binding energies, which corresponded to poses inconsistent with the initial model of binding of compound 5 to PEX14 (PDB accession code: 7QRC). This consisted primarily of flips of the tricyclic scaffold to expose the terminal benzene ring to the solvent. We chose the poses with the lowest QM binding energy for our analysis. This means, e.g., that for the carboxamide derivatives, only the models in which we observed interactions with the two solvation water molecules remained after the curation and selection protocol. The docking poses were visualized in PyMol [40].

# 4.2.3. EDDA calculations

EDDA is a QM-based partition scheme that calculates and factorizes binding energies over several components, each of which is associated with a specific physicochemical force: electrostatic interactions (ES), polarization (POL), charge transfer (CT), lipophilicity or dispersion (DISP), steric hindrance or electronic repulsion (REP), and solvation contributions (SOLV). All these terms are additive and sum up to the interaction or binding energy (INT). Because the binding energy correlates with the binding enthalpy, this partitioning identifies the driving forces that lead to binding. When analyzing trends of matched molecular pairs: 1) we present column plots of the decomposed energies of reference compounds (equivalent to an electronic pharmacophore model); 2) we discuss matched molecular pairs using differential EDDA column plots. The latter correspond to differences in each energy contribution between a ligand and the reference compound. This simplifies understanding the fine networks of chemical interactions leading to protein binding. For the structural interpretation of the results, each energy contribution is further deconvoluted over atomic contributions. Those are represented in the form of maps, which illustrate detailed contributions of the ligand's atoms for each specific interaction with a protein. In the maps, the blue color is used to represent attractive interactions, whereas red indicates repulsive atomic contacts. The size of each sphere correlates with the strength of the respective interaction. The EDDAs were performed for a single structure that resulted from the selection protocol described in section 4.2.2. The calculations were run using the ULYSSES package [41] as previously reported [42,43]. The quantum mechanical Hamiltonian chosen for the calculations was GFN2-xTB [44], as this proved to be accurate enough for estimating relative binding data [45]. Note that GFN2-xTB has its own, specific basis set due to its semi-empirical nature. To better reproduce solvation effects, we supplemented the two explicit water molecules in the model with implicit water solvation [46]. The maps were generated using a Python script and visualized using ChimeraX [47]. All maps are provided in the Supporting Data.

# 4.2.4. SAR analysis workflow

The computational workflow we applied was the following.

- 1) Prepare the crystal structure for docking experiments.
- Prepare the structures of all inhibitors we wish to study in the.sdf format.

- Use Schrodinger's Maestro to dock all ligands, requesting the ten best-scoring binding poses.
- 4) Run the EDDA calculations on each generated complex.

Each EDDA calculation currently requires up to 3 days of computing time for systems with up to 5000 atoms, and if the protein's charge and protonation state are correct (no radicals). In the case of PEX14, with *ca.* 1200 atoms, all calculations required less than 6 h of computing time. This means that no protein had to be clipped for the present work. We also stress that using up to 5000 atoms yields converged energetics for most systems we studied.

5) We excluded all structures with less favorable binding energetics to parse the computational data according to the QM calculations. For further analysis, we selected the poses with the lowest binding energy. These were kept, except when the ligand exhibits an overly distorted and unrealistic binding pose.

The QM-EDDA binding energies are equivalent to a quantum mechanical MMGBSA scoring function. We stress that the QM-EDDA only scores structures computationally and lacks any "generative" or sampling power. This is left to the discretion of users, who need to generate binding poses using alternative means (in our case, this was Schrodinger's Maestro). Though the QM basis offers better energetics than a traditional MMGBSA approach, the speed with which calculations are run limits the conformational spaces sampled. Nonetheless, we stress that using Boltzmann statistics limits the number of conformers needed to describe each complex.

### 4.3. Protein expression and purification

The N-terminal domain of *Tb*PEX14 (aa 19–84) was cloned into pETM-11 (EMBL). The plasmids were transformed into *E. coli* BL21. 5 ml of the overnight culture was inoculated in 500 ml of the autoinduction medium [48] supplemented with 50 µg/mL of kanamycin. When the cell density (OD600) reached 0.8, the temperature was lowered to 18 °C, and the cells were grown overnight. The cells were harvested by centrifugation and dissolved in lysis buffer (50 mM Tris pH 8.0, 300 mM NaCl, 10 mM  $\beta$ -mercaptoethanol, 20 mM imidazole, 10 mg/ml DNAsel, 1 mM AEBSF) and lysed by sonication. The lysates, clarified by centrifugation, were passed over a Ni-NTA agarose resin (Qiagen, Germany) pre-equilibrated with buffer A (50 mM Tris pH 8.0, 300 mM NaCl, 10 mM  $\beta$ -mercaptoethanol, 20 mM imidazole) and the protein of interest was eluted with the same buffer containing 250 mM imidazole. The concentrated eluates were further purified on a Superdex 75 Hiload 16/60 column (GE Healthcare) in phosphate-buffered saline (PBS).

# 4.4. Biophysical assays

### 4.4.1. AlphaScreen assay

According to the published protocol, the AlphaScreen assay was used to derive the half-maximal effective concentration (EC50) values for the PEX5-TbPEX14 inhibitors [20]. 3 nM N-His-PEX14 was mixed with 10 nM biotinylated PEX5-derived peptide (ALSENWAQEFLA) in PBS supplemented with 5 mg/mL of BSA and 0.01 % (v/v) Tween-20. 5  $\mu$ g/mL of streptavidin donor beads and 5  $\mu g/mL$  of nickel chelate acceptor beads (PerkinElmer) were added to the mixture. The serial dilutions of the inhibitors were prepared in DMSO and mixed while keeping the concentration of DMSO constant (5 %; this concentration was shown not to effect the assay readout). The competition curves were measured using a serial dilution of the inhibitor while keeping the concentrations of all other assay components constant. Data were measured in quadruplicate. The inhibitor  $EC_{50}$  was calculated from the Hill sigmoidal fitting, fixing the asymptotes at the maximal assay signal (no inhibitor added) and 0, respectively. The signal was determined according to the bead manufacturer instructions. The data were analyzed using Origin

Pro 9.0 [49].

# 4.4.2. <sup>1</sup>H, <sup>15</sup>N HSQC NMR

Compound 7 and 37 binding to PEX14 was monitored with  $^1\text{H},^{15}\text{N}$  2D correlation spectra on a Bruker Avance III 600 MHz spectrometer ( $^1\text{H}$  frequency 600 MHz) with a QCI cryoprobe. Samples were made up with 200  $\mu\text{M}$  uniformly  $^{15}\text{N}$ -labeled TbPEX14 protein in phosphate NMR buffer (pH 6.5, 20 mM NaCl, 5 mM Na<sub>x</sub>PO<sub>4</sub>) in water, supplemented with 10 % D<sub>2</sub>O. Compounds were dissolved in DMSO- $d_6$  and aliquots were added to the test samples at appropriate ligand to protein concentration ratio and DMSO- $d_6$  was added to the reference sample.

# 4.5. Cellular assays

# 4.5.1. In vitro trypanocidal activity of compounds against T. b. brucei

T. b. brucei bloodstream form (Lister 427, MITat 1.2) parasites were grown in a HMI-11 medium [50] containing 10 % fetal bovine serum (FBS) at 37 °C with 5 % CO2. Anti-trypanosomal activities of the compounds were tested using a resazurin-based 96-well plate assay. Twofold serial dilutions of each compound (10 wells in each row) were prepared in 96-well plates in HMI-11 medium (100 µL/well, quadruplicates). As controls, each row included a well without compound and a well with medium alone. 100  $\mu$ L of parasite cultures (4 × 10<sup>3</sup>/mL) were inoculated in all wells, except in the well with media alone. Final concentration of parasites was  $2 \times 10^3$ /mL. The plates were incubated for 66 h. Resazurin (25 µL of 0.1 mg/mL in Hank's Balanced Salt Solution) was added to all wells, and the plates were further incubated until the 72 h timepoint. Resazurin reduction by living cells was quantified by measuring the fluorescence with a Synergy H1 microplate reader (excitation 530 nm, emission 585 nm). After subtracting the background fluorescence of the well with media alone, percentual survival values were calculated by setting the fluorescence of the wells without compound to "100 % survival". Nonlinear regression graphs were plotted in GraphPad Software GraphPad Prism 10 [51] to yield sigmoidal dose-response curves, and half-maximal effective concentration (EC<sub>50</sub>) values were determined.

# 4.5.2. Cytotoxicity of compounds against HepG2 cells

HepG2 (Hepatocyte) cells were seeded in 96-well plates (5000 cells/well in rows B–H) and grown overnight at 37 °C in a humidified incubator with 5 % CO<sub>2</sub>. Compounds were tested in triplicate from 100 to 3.125  $\mu M$  (twofold serial dilutions, from row H to row C). Row A contained medium alone and served as a negative control. Row B contained cells alone without inhibitors and served as a positive control. Hygromycin B (InvivoGen) was used as a positive control for cytotoxicity. After incubation for 66 h, 25  $\mu L$  of 0.1 mg/mL resazurin (dissolved in Hanks Balanced Salt Solution HBSS, Sigma) was added to all wells. Plates were further incubated for 6 h. Fluorescence was measured, and the data were processed as described above for the *T. b. brucei* cytotoxicity assay.

# CRediT authorship contribution statement

Michał Nowacki: Writing – review & editing, Writing – original draft, Validation, Supervision, Methodology, Investigation, Data curation, Conceptualization. Filipe Menezes: Writing – review & editing, Writing – original draft, Visualization, Software, Methodology, Data curation, Conceptualization. Emilia Pykacz: Writing – review & editing, Investigation. Mateusz Popiołek: Investigation. Valeria Napolitano: Writing – review & editing, Methodology, Investigation, Data curation. Chethan K. Krishna: Writing – review & editing, Investigation, Data curation. Vishal C. Kalel: Writing – review & editing, Supervision, Resources, Methodology, Investigation, Data curation. Ralf Erdmann: Writing – review & editing, Supervision, Resources, Methodology, Funding acquisition. Tony Fröhlich: Software, Investigation, Data curation. Oliver Plettenburg: Writing – review & editing, Supervision, Funding acquisition. Michael Sattler: Writing – review &

editing, Resources, Methodology, Funding acquisition, Conceptualization. Grzegorz M. Popowicz: Writing – review & editing, Resources, Methodology, Funding acquisition, Conceptualization. Maciej Dawidowski: Writing – review & editing, Writing – original draft, Visualization, Supervision, Resources, Project administration, Methodology, Investigation, Funding acquisition, Data curation, Conceptualization.

# Declaration of competing interest

The authors declare that they have no known competing financial interests or personal relationships that could have appeared to influence the work reported in this paper.

### Acknowledgments

This study has been funded by Narodowe Centrum Nauki (grant 2018/31/B/NZ7/02089 to M.N., E.P. and M.D.), by Ruhr University Bochum, InnovationsFoRUM (Host Microbe Interactions: IF-009N-22 and IF-018N-22 to R.E.), by Bundesministerium für Bildung und Forschung (grant PEXMED to G.P., M.S. and R.E.), by Deutsche Forschungsgemeinschaft (grant Transregio 387 to G.P. and O.P.), and by Bundesministerium für Wirtschaft und Klimaschutz (grant KK5710001BA4 to F.M.).

# Appendix A. Supplementary data

Supplementary data to this article can be found online at https://doi. org/10.1016/j.ejmech.2025.117979.

### Data availability

Data will be made available on request.

# References

- H. Nada, Y. Choi, S. Kim, K.S. Jeong, N.A. Meanwell, K. Lee, New insights into protein–protein interaction modulators in drug discovery and therapeutic advance, Signal Transduct. Targeted Ther. 9 (2024) 341.
- [2] A. Mullard, Protein-protein interaction inhibitors get into the groove, Nat. Rev. Drug Discov. 11 (2012) 173–175.
- [3] R. Zhang, Y. Zheng, F. Xiang, J. Zhou, Inducing or enhancing protein-protein interaction to develop drugs: molecular glues with various biological activity, Eur. J. Med. Chem. 277 (2024) 116756.
- [4] J.F. Greenblatt, B.M. Alberts, N.J. Krogan, Discovery and significance of proteinprotein interactions in health and disease, Cell 187 (2024) 6501–6517.
- [5] D.E. Scott, A.R. Bayly, C. Abell, J. Skidmore, Small molecules, big targets: drug discovery faces the protein–protein interaction challenge, Nat. Rev. Drug Discov. 15 (2016) 533–550.
- [6] D. Valenti, S. Hristeva, D. Tzalis, C. Ottmann, Clinical candidates modulating protein-protein interactions: the fragment-based experience, Eur. J. Med. Chem. 167 (2019) 76–95.
- [7] D. Wu, Y. Li, L. Zheng, H. Xiao, L. Ouyang, G. Wang, Q. Sun, Small molecules targeting protein–protein interactions for cancer therapy, Acta Pharm. Sin. B 13 (2023) 4060–4088.
- [8] V. Marković, A. Szczepańska, Ł. Berlicki, Antiviral protein-protein interaction inhibitors, J. Med. Chem. 67 (2024) 3205–3231.
- [9] P. Buchwald, Developing small-molecule inhibitors of protein-protein interactions involved in viral entry as potential antivirals for COVID-19, Front. Drug Discover. 2 (2022).
- [10] A.A. Thompson, M.B. Harbut, P.-P. Kung, N.K. Karpowich, J.D. Branson, J.C. Grant, D. Hagan, H.A. Pascual, G. Bai, R.B. Zavareh, H.R. Coate, B.C. Collins, M. Côte, C. F. Gelin, K.L. Damm-Ganamet, H. Gholami, A.R. Huff, L. Limon, K.J. Lumb, P. A. Mak, K.M. Nakafuku, E.V. Price, A.Y. Shih, M. Tootoonchi, N.A. Vellore, J. Wang, N. Wei, J. Ziff, S.B. Berger, J.P. Edwards, A. Gardet, S. Sun, J.E. Towne, J. D. Venable, Z. Shi, H. Venkatesan, M.-L. Rives, S. Sharma, B.T. Shireman, S. J. Allen, Identification of small-molecule protein—protein Interaction Inhibitors for NKG2D, vol 120, Proceedings of the National Academy of Sciences, 2023 e2216342120.
- [11] M.D. Andrews, K.N. Dack, M.J. de Groot, M. Lambert, C.J. Sennbro, M. Larsen, M. Stahlhut, Discovery of an oral, rule of 5 compliant, interleukin 17A protein–protein interaction modulator for the potential treatment of psoriasis and other inflammatory diseases, J. Med. Chem. 65 (2022) 8828–8842.
- [12] Y. Zheng, C.H. Kan, T.F. Tsang, Y. Liu, T. Liu, M.W. Tsang, L.Y. Lam, X. Yang, C. Ma, Discovery of inhibitors targeting protein–protein interaction between

- bacterial RNA polymerase and NusG as novel antimicrobials, J. Med. Chem.  $67(2024)\ 16556-16575$ .
- [13] A. Kaplan, B. Morquette, A. Kroner, S. Leong, C. Madwar, R. Sanz, S.L. Banerjee, J. Antel, N. Bisson, S. David, A.E. Fournier, Small-molecule stabilization of 14-3-3 protein-protein interactions stimulates axon regeneration, Neuron 93 (2017) 1082–1093.e1085.
- [14] A. Abidi, P. Shukla, A. Ahmad, Lifitegrast: a novel drug for treatment of dry eye disease, J. Pharmacol. Pharmacother. 7 (2016) 194–198.
- [15] E.D. Deeks, Venetoclax: first global approval, Drugs 76 (2016) 979-987.
- [16] S.C. Bukow, M. Daffertshofer, M.G. Hennerici, Tirofiban for the treatment of ischaemic stroke, Expet Opin. Pharmacother. 7 (2006) 73–79.
- ischaemic stroke, Expet Opin. Pharmacother. 7 (2006) 73–79. [17] S. Dhillon, Carotegrast methyl: first approval, Drugs 82 (2022) 1011–1016.
- [18] X. Xie, T. Yu, X. Li, N. Zhang, L.J. Foster, C. Peng, W. Huang, G. He, Recent advances in targeting the "undruggable" proteins: from drug discovery to clinical trials, Signal Transduct. Targeted Ther. 8 (2023) 335.
- [19] Michelle R. Arkin, Y. Tang, James A. Wells, Small-molecule inhibitors of proteinprotein interactions: progressing toward the reality, Chem. Biol. 21 (2014) 1102–1114.
- [20] M. Dawidowski, L. Emmanouilidis, V.C. Kalel, K. Tripsianes, K. Schorpp, K. Hadian, M. Kaiser, P. Mäser, M. Kolonko, S. Tanghe, A. Rodriguez, W. Schliebs, R. Erdmann, M. Sattler, G.M. Popowicz, Inhibitors of PEX14 disrupt protein import into glycosomes and kill trypanosoma parasites, Science 355 (2017) 1416–1420.
- [21] C. Neufeld, F.V. Filipp, B. Simon, A. Neuhaus, N. Schüller, C. David, H. Kooshapur, T. Madl, R. Erdmann, W. Schliebs, M. Wilmanns, M. Sattler, Structural basis for competitive interactions of Pex14 with the import receptors Pex5 and Pex19, EMBO J. 28 (2009) 745–754, 754.
- [22] M. Dawidowski, V.C. Kalel, V. Napolitano, R. Fino, K. Schorpp, L. Emmanouilidis, D. Lenhart, M. Ostertag, M. Kaiser, M. Kolonko, B. Tippler, W. Schliebs, G. Dubin, P. Mäser, I.V. Tetko, K. Hadian, O. Plettenburg, R. Erdmann, M. Sattler, G. M. Popowicz, Structure–activity relationship in Pyrazolo[4,3-c]pyridines, first inhibitors of PEX14–PEX5 protein–protein interaction with trypanocidal activity, J. Med. Chem. 63 (2020) 847–879.
- [23] R. Fino, D. Lenhart, V.C. Kalel, C.A. Softley, V. Napolitano, R. Byrne, W. Schliebs, M. Dawidowski, R. Erdmann, M. Sattler, G. Schneider, O. Plettenburg, G. M. Popowicz, Computer-aided design and synthesis of a new class of PEX14 inhibitors: substituted 2,3,4,5-Tetrahydrobenzo[f][1,4]oxazepines as potential new trypanocidal agents, J. Chem. Inf. Model. 61 (2021) 5256–5268.
- [24] M. Marciniak, P. Mróz, V. Napolitano, V.C. Kalel, R. Fino, E. Pykacz, W. Schliebs, O. Plettenburg, R. Erdmann, M. Sattler, G.M. Popowicz, M. Dawidowski, Development of novel PEX5-PEX14 protein-protein interaction (PPI) inhibitors based on an oxopiperazine template, Eur. J. Med. Chem. 258 (2023) 115587.
- [25] E.L. Ratkova, M. Dawidowski, V. Napolitano, G. Dubin, R. Fino, M.S. Ostertag, M. Sattler, G. Popowicz, I.V. Tetko, Water envelope has a critical impact on the design of protein–protein interaction inhibitors, Chem. Commun. 56 (2020) 4360–4363.
- [26] M. Pelay-Gimeno, A. Glas, O. Koch, T.N. Grossmann, Structure-based design of inhibitors of protein–protein interactions: mimicking peptide binding epitopes, Angew. Chem. Int. Ed. 54 (2015) 8896–8927.
- [27] A. Yasgar, A. Jadhav, A. Simeonov, N.P. Coussens, AlphaScreen-Based assays: ultra-high-throughput screening for small-molecule inhibitors of challenging enzymes and protein-protein interactions, in: W.P. Janzen (Ed.), High Throughput Screening: Methods and Protocols, Springer New York, New York, NY, 2016, pp. 77–98.
- [28] V. Napolitano, P. Mróz, M. Marciniak, V.C. Kalel, C.A. Softley, J.D. Janna Olmos, B. G. Tippler, K. Schorpp, S. Rioton, T. Fröhlich, O. Plettenburg, K. Hadian, R. Erdmann, M. Sattler, G.M. Popowicz, M. Dawidowski, G. Dubin, Structure-based design, synthesis and evaluation of a novel family of PEX5-PEX14 interaction inhibitors against trypanosoma, Eur. J. Med. Chem. 243 (2022) 114778.
- [29] A. Dömling, W. Wang, K. Wang, Chemistry and biology of multicomponent reactions, Chem. Rev. 112 (2012) 3083–3135.

- [30] R.A. Bunce, J.E. Schammerhorn, Dibenzo-fused seven-membered nitrogen heterocycles by a tandem reduction-lactamization reaction, J. Heterocycl. Chem. 43 (2006) 1031–1035.
- [31] M. Billamboz, F. Bailly, P. Cotelle, Facile synthesis of 4-alkoxycarbonylisoquinoline-1,3-diones and 5-alkoxycarbonyl-2-benzazepine-1,3-diones via a mild alkaline cyclization, J. Heterocycl. Chem. 46 (2009) 392–398.
- [32] R.A. Bunce, J.E. Schammerhorn, A synthesis of selected 0,0'-disubstituted diarylacetic esters and diarylmethanes, Org. Prep. Proced. Int. 37 (2005) 550–555.
- [33] D.J. Bull, M.J. Fray, M.C. Mackenny, K.A. Malloy, Facile decarboxylation of nitrobenzeneacetic acids as a convenient route to alkylnitrobenzenes, Synlett 1996 (1996) 647–648.
- [34] G.A. Boyle, T. Govender, H.G. Kruger, G.E.M. Maguire, Synthesis of chiral pentacyclo-undecane ligands and their use in the enantioselective alkylation of benzaldehyde with diethylzinc, Tetrahedron Asymmetry 15 (2004) 2661–2666.
- [35] J. Firl, W. Maier, H. Daake, Synthese und Reaktionen des 6,11-Dihydro-5H-pyrido [3,2-c]-[1] benzazepin-5-ons, Liebigs Ann. Chem. 1989 (1989) 469-475.
- [36] S. Lee, H.-J. Lim, K.L. Cha, G.A. Sulikowski, Asymmetric approaches to 1,2disubstituted mitosenes based on the intramolecular cyclization of diazoesters, Tetrahedron 53 (1997) 16521–16532.
- [37] Schrödinger Release 2021-2: Maestro 12-8.117, Schrödinger, LLC, New York, NY, 2025
- [38] M.D. Hanwell, D.E. Curtis, D.C. Lonie, T. Vandermeersch, E. Zurek, G.R. Hutchison, Avogadro: an advanced semantic chemical editor, visualization, and analysis platform, J. Cheminf. 4 (2012) 17.
- [39] R.A. Friesner, R.B. Murphy, M.P. Repasky, L.L. Frye, J.R. Greenwood, T.A. Halgren, P.C. Sanschagrin, D.T. Mainz, Extra precision glide: docking and scoring incorporating a model of hydrophobic enclosure for protein—ligand complexes, J. Med. Chem. 49 (2006) 6177–6196.
- [40] The Pymol Molecular Graphics System, Version 2.5.7., in, Schrödinger, LLC.
- [41] F. Menezes, G.M. Popowicz, ULYSSES: an efficient and easy to use semiempirical library for C++, J. Chem. Inf. Model. 62 (2022) 3685–3694.
- [42] P. Grygier, K. Pustelny, J. Nowak, P. Golik, G.M. Popowicz, O. Plettenburg, G. Dubin, F. Menezes, A. Czarna, Silmitasertib (CX-4945), a clinically used CK2-Kinase inhibitor with additional effects on GSK3β and DYRK1A kinases: a structural perspective, J. Med. Chem. 66 (2023) 4009–4024.
- [43] I. Góral, T. Wichur, E. Sługocka, P. Grygier, M. Głuch-Lutwin, B. Mordyl, E. Honkisz-Orzechowska, N. Szałaj, J. Godyń, D. Panek, P. Zaręba, A. Sarka, P. Žmudzki, G. Latacz, K. Pustelny, A. Bucki, A. Czarna, F. Menezes, A. Więckowska, Exploring novel GSK-3β inhibitors for anti-neuroinflammatory and neuroprotective effects: synthesis, crystallography, computational analysis, and biological evaluation, ACS Chem. Neurosci. 15 (2024) 3181–3201.
- [44] C. Bannwarth, S. Ehlert, S. Grimme, GFN2-xTB—an accurate and broadly parametrized self-consistent tight-binding quantum chemical method with multipole electrostatics and density-dependent dispersion contributions, J. Chem. Theor. Comput. 15 (2019) 1652–1671.
- [45] P. Grygier, K. Pustelny, F. Menezes, M. Jemiola-Rzeminska, P. Suder, G. Dubin, A. Czarna, Structural perspective on the design of selective DYRK1B inhibitors, structural perspective on the design of selective DYRK1B inhibitors, bioRxiv (2022), 12.23.521429.
- [46] S. Ehlert, M. Stahn, S. Spicher, S. Grimme, Robust and efficient implicit solvation model for fast semiempirical methods, J. Chem. Theor. Comput. 17 (2021) 4250–4261.
- [47] E.C. Meng, T.D. Goddard, E.F. Pettersen, G.S. Couch, Z.J. Pearson, J.H. Morris, T. E. Ferrin, UCSF ChimeraX: tools for structure building and analysis, Protein Sci. 32 (2023) e4792
- [48] F.W. Studier, Protein production by auto-induction in high-density shaking cultures, Protein Expr. Purif. 41 (2005) 207–234.
- [49] OriginPro, 9.0, in, Originlab Corporation, Northampton, MA, USA.
- [50] H. Hirumi, K. Hirumi, Continuous cultivation of Trypanosoma brucei blood stream forms in a medium containing a low concentration of serum protein without feeder cell lavers. J. Parasitol. 75 (1989) 985–989.
- [51] Graphpad Prism 10, GraphPad Software, Inc, San Diego, CA, USA.